Journal of Power Sources 662 (2026) 238793

Contents lists available at ScienceDirect

Journal of Power Sources

journal homepage: www.elsevier.com/locate/jpowsour

Review article

Pinhole formation in proton exchange membrane in fuel cells: Degradation mechanisms and mitigation strategies

Cam-Tu Hoang-Ngoc, Sang Moon Kim *

Department of Mechanical Engineering, Incheon National University, Incheon, 22012, Republic of Korea

HIGHLIGHTS

- Pinhole in PEMFC membranes from through chemical, mechanical, thermal degradation.
- Defects cause gas crossover, efficiency loss, mechanical failure, and safety risks.
- Imaging, electrochemical, and gas-based tools enable early, reliable detection.
- Mitigation uses self-healing ionomers, composites, surface mods, and AI-assisted.
- Integrated, multifunctional designs aim to meet DOE durability targets.

GRAPHICAL ABSTRACT

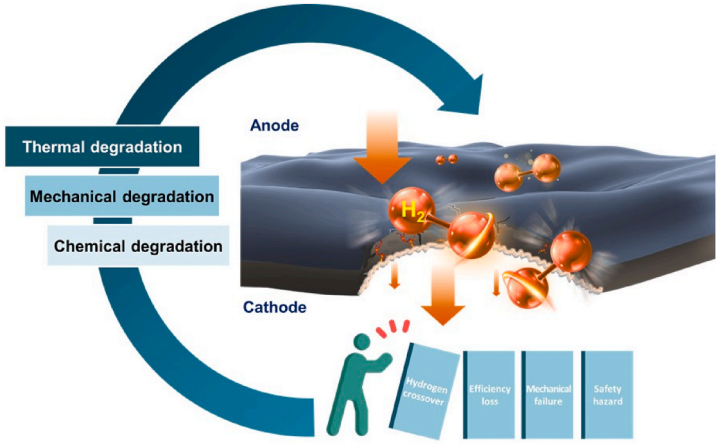

ARTICLE INFO

Keywords:
Pinhole
Degradation
PEMFC
Membrane
Diagnostics

ABSTRACT

The long-term durability of proton exchange membranes (PEMs) remains a major challenge to the commercialization of proton exchange membrane fuel cells (PEMFCs). Among various failure modes, pinhole formation has been identified as a critical degradation pathway that leads to gas crossover, performance loss, and a shortened device lifespan. This review provides a state-of-the-art understanding of how chemical, mechanical, and thermal stressors nucleate and propagate pinholes, emphasizing the strong synergies between these degradation modes under realistic operating conditions. Recent advances in diagnostic techniques capable of detecting incipient defects are critically compared. Emerging mitigation strategies—including self-healing ionomers, composite reinforcements, surface modifications, and radical-scavenging chemistries—are systematically discussed alongside simulation- and artificial-intelligence-assisted approaches, which enable predictive analysis and data-driven design of durable membranes. This review concludes by identifying remaining knowledge gaps, recommending standardized accelerated-stress-test protocols, and outlining material-design pathways towards next-generation, pinhole-resistant PEMs capable of meeting the U.S. Department of Energy's durability target and beyond.

* Corresponding author.
E-mail address: ksm7852@inu.ac.kr (S.M. Kim).

https://doi.org/10.1016/j.jpowsour.2025.238793
Received 27 August 2025; Received in revised form 10 October 2025; Accepted 5 November 2025
Available online 12 November 2025

List of Abbreviations

AEMs	Anion exchange membranes
AST	Accelerated stress testing
CL	Catalyst layer
C–O–C	Ether linkages
-COOH	Carboxylic acid groups
C-S	Carbon sulfur
CV	Cyclic voltammetry
DOE	United States Department of Energy
EIS	Electrochemical impedance spectroscopy
e-PTFE	Expanded polytetrafluoroethylene
FIB-SEM	Focused ion beam-scanning electron microscopy
FT	Fault Tree
GDL	Gas diffusion layer
H_2O_2	Hydrogen peroxide
HFR	High-frequency resistance
IR	Infrared
IRT	Infrared thermography
LSC	Long side-chain
LSV	Linear sweep voltammetry
MEA	Membrane electrode assemblies
MPL	Microporous layer
OCV	Open circuit voltage
•OH	Hydroxyl radicals
OM	Optical microscopy
PEMFCs	Proton exchange membrane fuel cells
PEMs	Proton exchange membranes
PFSA	Perfluorosulfonic acid
RH	Relative humidity
ROS	Reactive oxygen species
SEM	Scanning electron microscopes
SGO	Sulfonated graphene oxide
-SO_3H	Sulfonic acid groups
SSC	Short side-chain

1. Background

Global decarbonization is urgent as energy demand rises and greenhouses-gas emissions persist, with Intergovernmental Panel on Climate Change (IPCC) and the International Energy Agency (IEA) warning current fossil trajectories miss climate stabilization targets [1,2]. This context underscores the critical need for clean, efficient, and environmentally friendly energy conversion technologies. Among the emerging solutions, Fuel cells have attracted increasing interest as clean energy conversion devices capable of generating electricity, heat, and water from hydrogen or other suitable fuels without combustion. The flexibility of fuel cell technology enables the conversion of clean hydrogen or other suitable fuels into electricity, heat, and water, allowing simultaneous utilization across various sectors and operational scenarios (Fig. 1a) [3]. Market momentum (Fig. 1b) accompanies rapid technical progress toward United States Department of Energy (DOE) targets for fuel cell efficiency, cost, and durability (Fig. 1c) [4]. Within the broader class of fuel cell technologies, proton exchange membrane fuel cells (PEMFCs) are especially notable for their combination of high energy density, scalability, rapid start-up, and relatively low operating temperatures (60–80 °C). These characteristics collectively underpin their suitability for diverse applications, ranging from residential energy systems to zero-emission vehicles and portable backup power [5–7]. Despite these advances, further improvements in material resilience are crucial for long-term performance and reliability, with electrolyte membrane durability remaining a key concern.

A schematic illustrating the operating principle of a PEMFC, shown in Fig. 1d, highlights the membrane's critical function in conducting protons from the anode to the cathode while simultaneously preventing the direct mixing of hydrogen and oxygen gases [8]. The membrane must therefore exhibit high proton conductivity, robust mechanical integrity, and chemical durability under diverse operating conditions [9]. In a typical fuel cell reaction, hydrogen at the anode dissociates into protons and electrons; protons traverse the membrane while electrons travel through an external circuit, generating useful electricity. As fuel cell technology advances beyond the laboratory and enters commercial markets, the durability of its core components becomes a determining factor for practical implementation. While steady improvements have been made in performance and cost, ensuring long-term membrane stability remains one of the most pressing challenges for PEMFCs.

Although polymer-based membranes include both proton exchange membranes (PEMs) and anion exchange membranes (AEMs), this review focuses exclusively on PEMs because the majority of commercial fuel cell applications employ PEM-based systems and research on AEMs remains comparatively limited. These include both perfluorosulfonic acid (PFSA)-based membranes, such as Nafion® and Aquivion®, which have been widely adopted in commercial fuel cells [10], and hydrocarbon-based PEMs, such as sulfonated poly(ether ether ketone) (SPEEK), sulfonated poly(arylene ether sulfone) (SPES), and polybenzimidazole (PBI), which are gaining increasing attention for their potential in cost reduction and high-temperature operation [11–14]. While these membrane families differ in polymer architecture, water uptake behavior, and operating conditions, they share common degradation stressors under fuel cell conditions. Moreover, pinhole formation has been observed across multiple PEM types, serving as a universal manifestation of membrane failure.

The DOE targets an 8000-h ultimate durability for automotive fuel cell systems [15], a benchmark remains difficult to meet in practice. Premature membrane failure directly impacts both system cost and operational reliability. The longevity of PEMs is diminished by a confluence of stressors [16,17], including exposure to reactive oxygen species (ROS), primarily generated during oxygen reduction, cyclic hydration and dehydration, thermal gradients, and mechanical compression [18–20]. These factors synergistically damage the membrane's chemical structure and physical integrity, leading to thinning, cracking, and ultimate failure. Among the various phenomena of degradation, pinhole formation, defined as the emergence of localized microscopic perforations through the membrane thickness, has recently been recognized as a particularly critical and underappreciated failure mode [21,22]. Pinholes are microscopic through-thickness defects, typically several to tens of micrometers (μm) in diameter, that locally breach gas separation and permit direct H_2/O_2 crossover. Unlike uniform thinning or large-area cracking, pinholes are highly localized failure sites that often arise where chemical attack and mechanical strain convergence [23–25]. In some cases, pinholes are initiated at the catalyst-membrane interface, where mechanical strain from humidity cycling converges with chemical degradation [25,26]. From a morphological perspective, pinholes are not static entities with gas-flow paths and membrane heterogeneity [27], and chemical fingerprints of degradation, notably carboxylic acid groups (-COOH), accumulate within ~150 μm of the epicenter, indicating radially expanding degradation zones [26,28].

To render the definition operational for testing, DOE durability anchors for combined chemical/mechanical stressors can be adopted: in linear sweep voltammetry (LSV)-based accelerated stress tests, failure is flagged at H_2 crossover $\geq$15 mA cm^{-2} or open circuit voltage (OCV) loss $\geq$20 % under the measurement conditions specified by the DOE protocol [29]. Although these thresholds do not themselves define a pinhole, they function as actionable proxies: sustained crossover increases accompanied by OCV decay are consistent with pinhole nucleation and growth, and OCV reduction can provide an early detection signal, as reported by Niroumand et al. [30]. Accordingly, pinhole-driven failure can be identified using a two-pronged criterion: (i) structural evidence (through-thickness perforation on imaging) and/or (ii) operational evidence (crossover/OCV exceeding the DOE anchors under the stated conditions).

Despite numerous studies addressing individual degradation pathways, such as radical-induced chain scission, hydration-driven cyclic swelling fatigue, or high-temperature dehydration [31–33], an integrated view of how these mechanisms interact to initiate and propagate pinholes remains limited. Critically, pinhole formation is not merely a

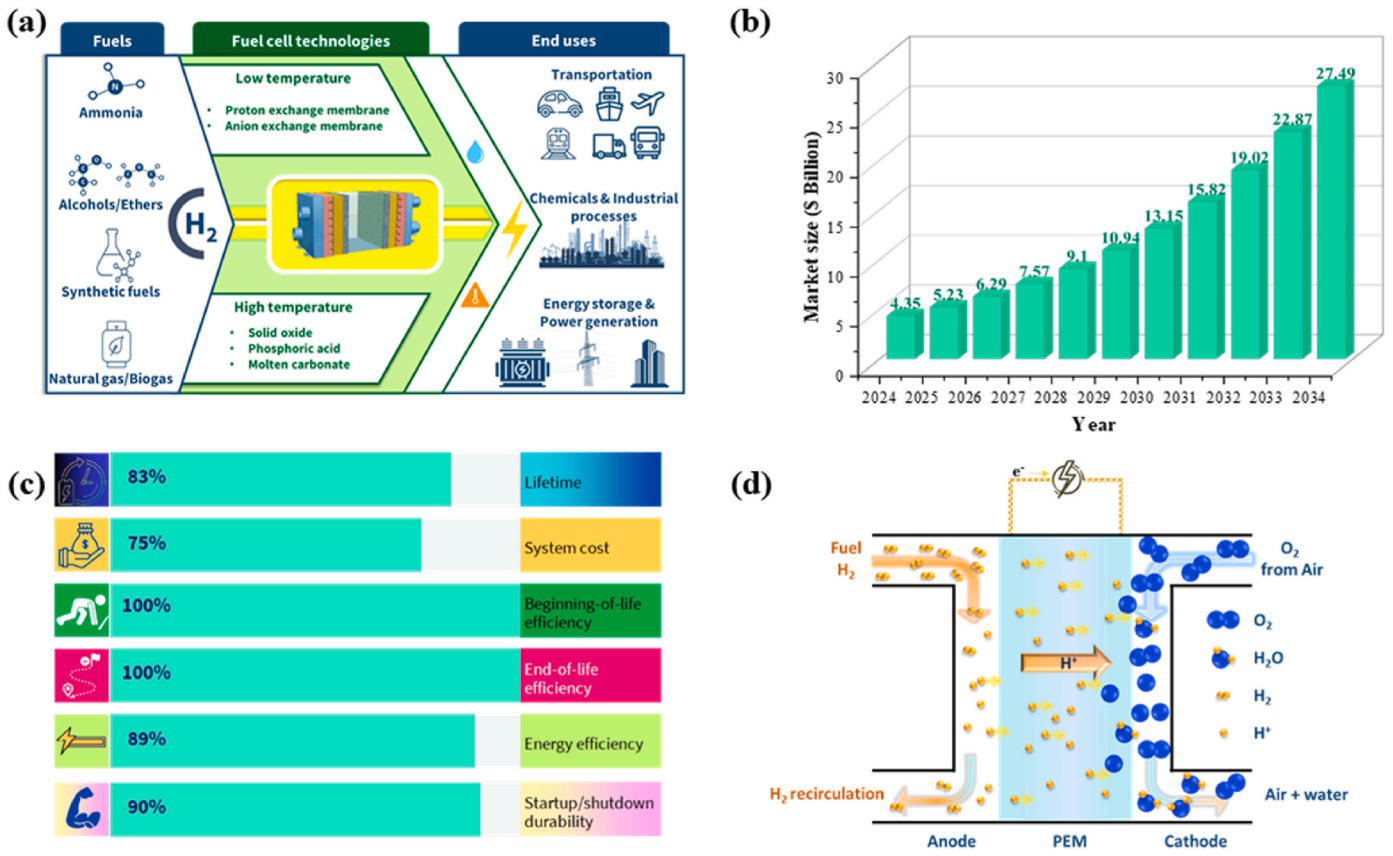

Fig. 1. (a) Fuel cell technologies converting clean hydrogen and other suitable fuels into electricity, heat, and water for diverse applications. (b) Global hydrogen fuel cell market size forecast between 2024 and 2034. (c) Progress toward DOE technical roadmap targets for efficiency, material utilization, and system optimization. (d) Schematic of the structure and operating principle of a proton exchange membrane fuel cell.

secondary consequence but rather a unique convergence points of multiple failure modes, representing a limiting factor in long-term PEMFC durability. The absence of a unified, mechanistic framework has hindered effective mitigation. This review addresses this gap through a comprehensive analysis of pinhole formation in proton exchange membranes, with emphasis on mechanistic origins, evolution from localized damage, and operational challenges. Recent advances in the understanding of chemical, mechanical, and thermal degradation processes are synthesized and linked to the generation and propagation of pinholes. In addition, state-of-the-art diagnostic tools for early pinhole detection are critically reviewed. Emerging material and design strategies aimed at mitigating this failure mode are systematically discussed. Finally, current limitations, knowledge gaps, and future research directions are outlined to advance the development of pinhole-resistant membranes for next-generation PEMFCs.

2. Classification of electrolyte membrane failure modes

The long-term durability of PEMFCs is intrinsically tied to the structural and functional stability of the electrolyte membrane. Although PEMFC degradation stems from multiple factors, including component aging as well as operational and environmental stressors, membrane integrity remains a decisive determinant of the fuel cell lifetime and reliability [34]. Operating under highly dynamic and often harsh electrochemical environments, the membrane is subjected to a combination of mechanical stress, thermal cycling, and chemical attack that accumulate over time [35].

To establish a clear foundation for later mechanistic discussions, this section presents a morphological classification of failure modes observed in proton exchange membranes. Unlike degradation mechanisms (detailed in Section 3), which focus on the origins and progression of damage, this classification is based on observable structural manifestations and functional consequences that impair or terminate membrane functionality. The most common failure modes include uniform thinning, pinhole formation, cracking and fracture, interfacial delamination, localized chemical decomposition zones, and channel formation - each representing distinct degradation pathways and severity levels (Fig. 2a). These failure modes are summarized in Table 1, which contrasts their morphological characteristics, operational consequences, reversibility, and typical contributing factors.

Although these failure modes can occur independently, they often overlap or evolve from one another. Notably, pinhole formation has emerged as a critical failure mode due to its irreversible nature and rapid impact on cell performance.

3. Mechanisms of pinhole formation and growth

In a PEMFC, each cell is composed of its core components arranged in a layered structure: bipolar plates, gas diffusion layers (GDLs), catalyst layers (CLs), and the PEM. Each of these components contributes to the overall electrochemical performance and mechanical integrity of the cell, yet they differ significantly in terms of degradation behavior and long-term durability. As illustrated in Fig. 2b, the membrane lies at the core of the membrane-electrode assembly (MEA), serving simultaneously as an ion conductor and a barrier to fuel crossover. Recent system-level analyses have confirmed the critical role of the PEM in governing fuel cell lifespan. Placca and Kouta [36] developed a Fault Tree (FT) model to estimate the degradation probability of PEMFCs under various operating conditions. Their approach integrates the failure probabilities of individual components to assess the likelihood of

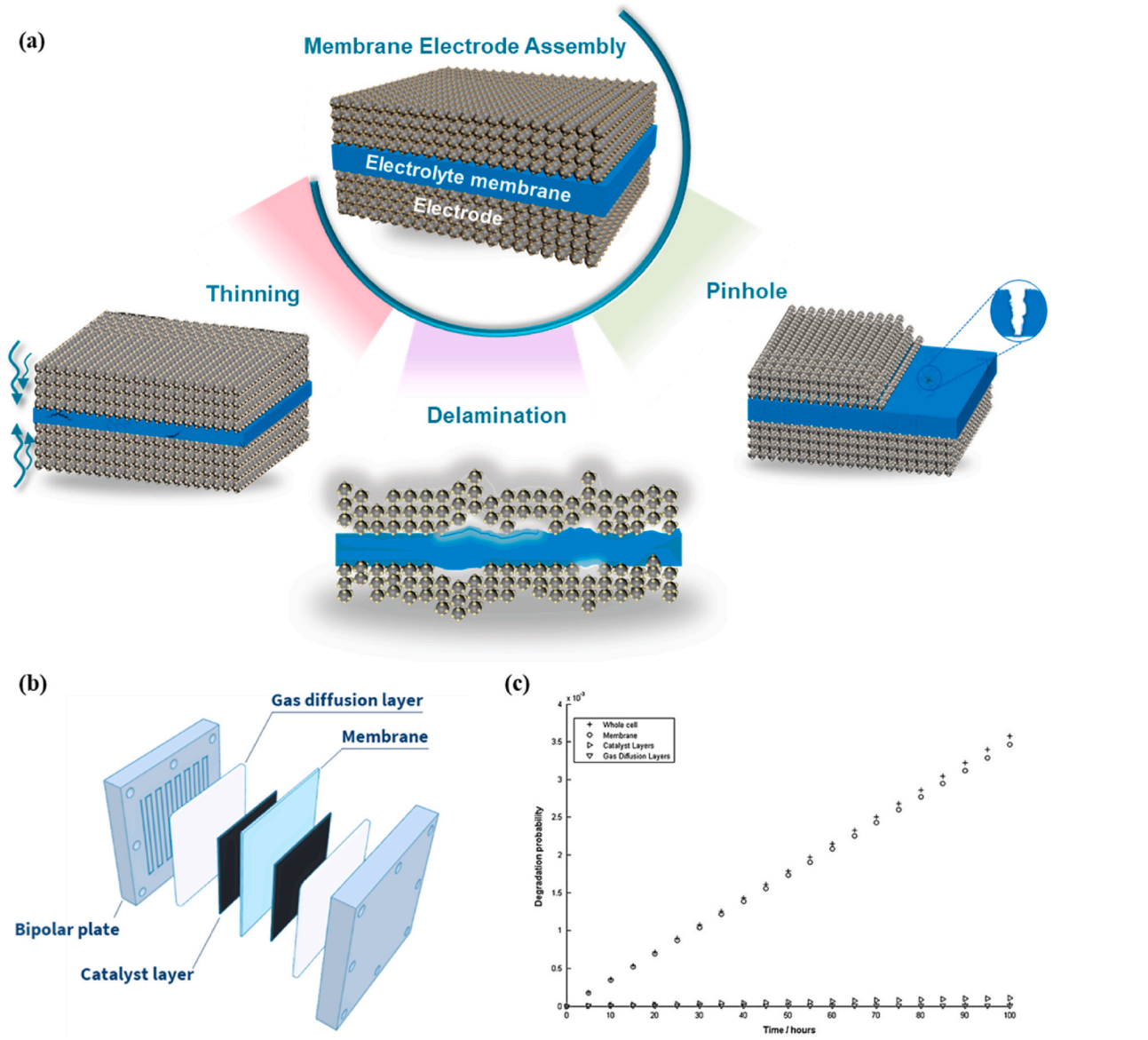

Fig. 2. (a) Schematic representation of the primary electrolyte membrane failure modes in PEM fuel cells: thinning, delamination, and pinhole formation. (b) Main components of a proton exchange membrane fuel cell. (c) Fault tree analysis illustrating the influence of each fuel cell component on the overall degradation probability. The PEM is identified as the most critical factor impacting system durability (adapted from Placca and Kouta [36]).

Table 1
Classification of typical electrolyte membrane failure modes in PEMFCs.

Failure mode	Morphology	Functional consequences	Reversibility	Common triggers	Ref.
Thinning	Gradual, homogeneous reduction in thickness	Decrease in conductivity and strength	Partially reversible	Radical attack, long-term chemical aging	[37,38]
Cracking & fracture	Visible fissures, partial or full-depth	Mechanical instability, precursor to pinholes	Mostly irreversible	Cyclic swelling fatigue, freeze-thaw	[39]
Interfacial delamination	Detachment between membrane and electrode	High local resistance, risk of drying or gas leakage	Reversible (in early stage)	Stress mismatch, weak adhesion	[40–42]
Localized decomposition zones	Discolored or embrittled regions	Loss of functional groups, precursor to cracking	Irreversible locally	ROS accumulation, dry out	[43–46]
Channel formation	Tunnel-like gas pathways	Severe gas crossover, current loss	Irreversible	Extended radical attack, extreme thermal aging	[34,47]
Pinhole formation	Microscopic through-thickness perforation	Gas crossover, voltage drop, cell failure	Irreversible	Chemical, mechanical, thermal synergy	[28,39]

overall system failure. As shown in Fig. 2c, the PEM was identified as the most critical component in determining fuel cell durability. In other words, once the membrane fails, the degradation of the entire cell is often inevitable.

The degradation of PEMs in fuel cells is a complex process influenced by a combination of intrinsic material properties and external operating

conditions. Among the most critical factors are chemical and mechanical stressors, the attack of reactive species-particularly hydroxyl radicals (•OH), the concentration of free radicals, and the nature of acidic functional groups within the polymer backbone. Repeated swelling and drying cycles induce mechanical fatigue and stress gradients that weaken the membrane structure over time. At elevated temperatures, dehydration accelerates both mechanical embrittlement and thermally induced scission reactions, especially at labile sites like ether linkages or sulfonic acid termini.

Importantly, these degradation mechanisms rarely act independently. In practical systems, they often operate in synergy: chemical damage weakens mechanical resilience, mechanical defects expose deeper regions to oxidative attack, and local heating exacerbates all failure modes [48]. This dynamic interplay not only shortens membrane lifetime but also accelerates the onset of pinholes, microscopic perforations that traverse both sides of the membrane. Pinhole formation is therefore best understood not as an isolated event, but as the cumulative endpoint of multiple degradation pathways converging over time. The

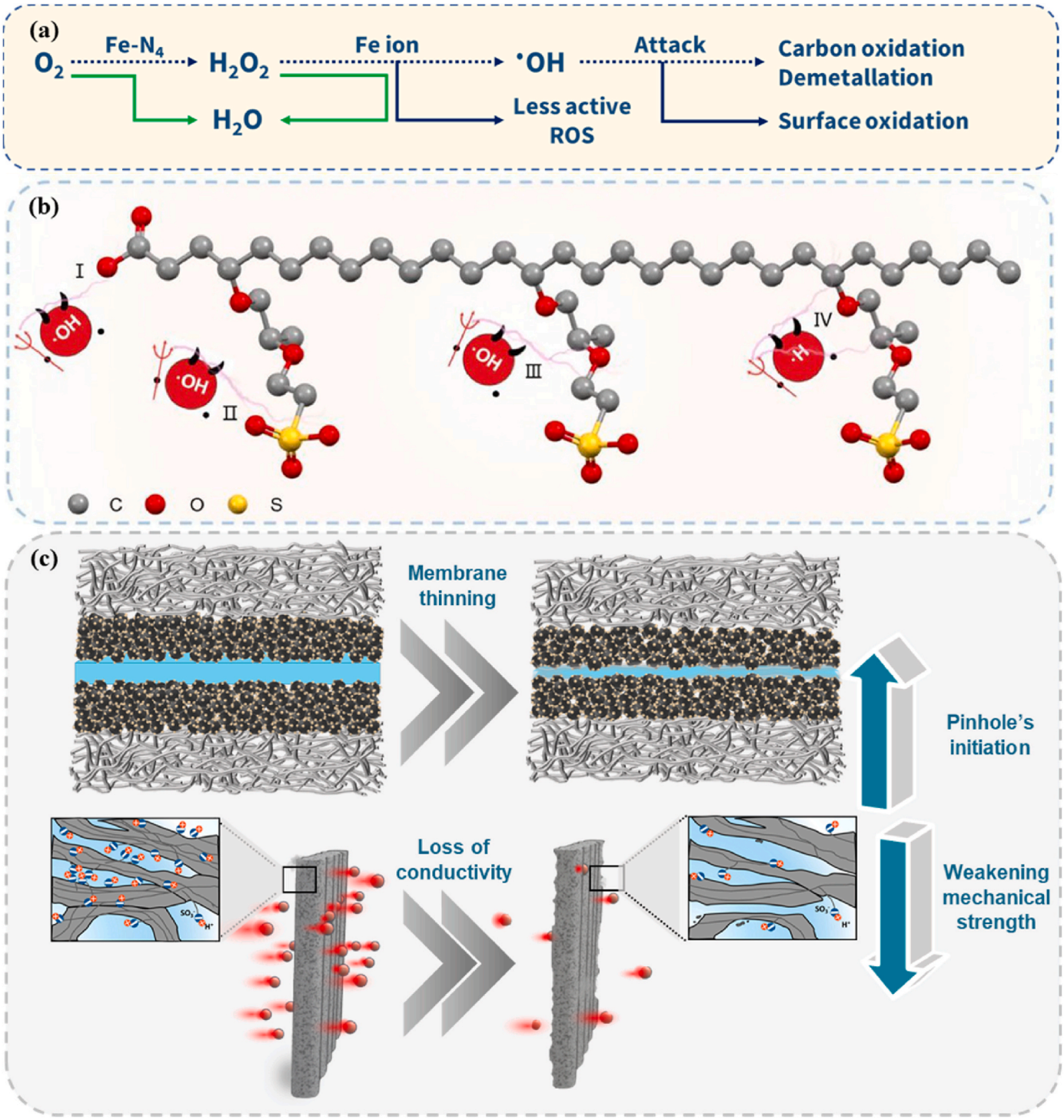

Fig. 3. a) Schematic of membrane degradation initiated by hydrogen peroxide generation and subsequent formation of reactive oxygen species near the catalyst layer. b) Radical-induced scission of polymer chains, leading to functional group loss and structural thinning associated with pinhole formation (adapted from Yu et al. [31]). (c) Consequential damage including severe conductivity loss, mechanical weakening, and initiation of pinholes as a result of cumulative chemical attack.

following subsections examine these pathways in greater detail, highlighting how chemical, mechanical, and thermal stressors initiate and propagate damage that ultimately manifests as pinholes in PEMFC membranes.

3.1. Chemical degradation

3.1.1. Radical formation and polymer breakdown

PEMs are typically synthesized through polymerization or chemical modification processes that yield a stable polymer backbone functionalized with acidic ion-conducting groups, most commonly sulfonic acid moieties, to ensure effective proton transport. Among the various types of PEMs, perfluorosulfonic acid (PFSA) membranes have remained the most widely adopted in PEMFCs, owing to their high proton conductivity, long-term electrochemical stability, and ease of processing. Notably, Nafion®, a commercial PFSA membrane with a Teflon-like fluorocarbon backbone and sulfonic acid side chains, continues to serve as a benchmark material due to its comprehensively studied performance and durability under fuel cell operating conditions. However, despite the inherent robustness of the PFSA structure, these membranes are vulnerable to chemical degradation of polymer chains, such as ether linkages (-OCF_2-) in the side chains and carbon sulfur (C-S) bonds near the sulfonic acid groups are susceptible to radical-induced attack, which can ultimately degrade the ion exchange capacity and structural integrity of the membrane. A representative degradation pathway is illustrated in Fig. 3a, and further elaborated in comprehensive reviews by Chen et al. and Shah et al. [49,50]. The degradation mechanism involves several steps: (1) Electrochemical formation of H_2O_2 via the two-electron oxygen reduction reactions at or near the catalyst layers. (2) Diffusion of H_2O_2 into the membrane matrix. (3) Decomposition of H_2O_2 into ROS, particularly •OH, via Fenton-type reactions catalyzed by transition metal ions such as Fe^{2+}. (4) Radical-induced attack on the membrane, targeting both the main chain and side chains. (5) Scission of polymer chains, leading to the detachment of functional groups and loss of polymer mass. (6) Degradation of the PFSA backbone, accompanied by fluoride and sulfur release and visible thinning or perforation of the membrane, as shown in Fig. 3b. The associated chemical equations are summarized in Table 2.

As the degradation process progresses, its consequences manifest not only at the molecular scale but also at the macroscopic performance level. Fig. 3c illustrates the cumulative outcomes of radical-induced damage, including significant loss of proton conductivity, mechanical weakening, and the initiation of microscopic pinholes. These effects are closely interrelated, leading to a decline in molecular weight that compromises the membrane's mechanical integrity, making it more vulnerable to stress-induced deformation. Recent quantitative analyses have confirmed the strong correlation between radical attack and measurable chemical degradation in PFSA membranes. Lee et al. [51] reported that under a combined chemical/mechanical accelerated stress test (AST) consisting of OCV holding at 95 °C and 30 % RH alternated with wet-dry cycling, the fluoride emission rate (FER) reached 0.0156 μmol h^{-1} cm^{-2} at the anode side and 0.0044 μmol h^{-1} cm^{-2} at the cathode side. This asymmetry reflects a higher probability of •OH radical generation near the anode, consistent with the Fe^{2+} catalyzed decomposition of H_2O_2. Concurrently, the membrane thickness decreased from 25 to 15 μm, the high-frequency resistance (HFR) dropped from 0.10 to 0.07 Ω cm^2, and the hydrogen crossover current density increased from 1 to > 40 mA cm^{-2}. The matching inflection points in FER, OCV decline, and crossover collectively demonstrate that chemical decomposition and mechanical fatigue synergistically accelerate structural failure and pinhole formation, providing direct experimental evidence linking radical-driven degradation to electrochemical performance loss.

Beyond fluoride emission, the decline in ion-exchange capacity (IEC) serves as another quantitative indicator of chemical aging. Curtin et al. [52] first demonstrated that fluoride release in PFSA membranes scales linearly with Fe^{2+} concentration in Fenton environments, and that pre-fluorinated Nafion® exhibited a 56 % reduction in F^- release after 50 h, confirming that backbone fluorination improves chemical resistance. Collier et al. [53] subsequently provided a comprehensive overview of radical-driven degradation, summarizing evidence that ROS such as •OH and •OOH attack both the polymer backbone and sulfonated side chains, leading to concurrent fluoride emission and IEC loss. Readers interested in the detailed kinetic interpretation are referred to their analysis. More recently, Sharma et al. [54] emphasized the link between IEC and membrane integrity: the number of ionizable –SO_3H groups, typically 0.91 meq•g^{-1} in pristine PFSA, decreased to 0.68 meq•g^{-1} after Fenton-type aging, accompanied by a proportional drop in proton conductivity. This quantitative relationship highlights the trade-off between maximizing IEC for proton transport and maintaining chemical and mechanical stability under radical-rich environments. Collectively, these studies reinforce that the combined quantification of fluoride release, IEC loss, and conductivity decline provides a robust framework for evaluating the chemical aging of PFSA membranes and linking molecular degradation to macroscopic durability.

Importantly, this degradation process is spatially heterogeneous and does not occur uniformly across the membrane. Mittal et al. [55] modeled H_2O_2 generation as most pronounced on the anode side due to lower potential and crossover gases [56–59]. Ohguri et al. [60] confirmed experimentally that •OH concentration is higher near the anode, consistent with the localized presence of Fe^{2+} ions. Additionally, reduced metal ions such as Fe^{2+} tend to remain more stable on the anode side, reinforcing the local conditions that favor radical formation [56]. Once •OH radicals are generated, they can initiate chain reactions that continuously shorten the polymer chains and release fluorine-containing fragments. These reactions are further accelerated at the interface between the catalyst layer and the membrane, where crossover gases and catalytic metals are in close proximity. A thorough molecular-level understanding of these mechanisms provides a foundation for developing effective mitigation strategies, such as the incorporation of metal scavengers [32,61,62], radical quenchers [63,64], or the design of next-generation membrane structures with enhanced resilience [65–67].

Table 2
Overview of the reactions involving free radicals in the process [50].

#	Reaction
1	$O_2 + 2H^+ + 2e\text{-} \rightarrow H_2O_2$, $\varphi^0 = 0.695$ V
2	$H_2O_2 \rightarrow 2HO\bullet$
3	$H_2O_2 + Fe^{2+} \rightarrow Fe^{3+} + HO\bullet + HO^-$
4	$H_2O_2 + Fe^{3+} \rightarrow Fe^{2+} + HOO\bullet + H^+$
5	$HO\bullet + Fe^{2+} \rightarrow HO\bullet + Fe^{3+}$
6	$HO\bullet + H_2O_2 \rightarrow HOO\bullet + H_2O$
7	$HO\bullet + O_2 \rightarrow HOO\bullet + H_2O$
8	$HOO\bullet + Fe^{3+} \rightarrow Fe^{2+} + H^+ + O_2$
9	$HOO\bullet + Fe^{2+} \rightarrow Fe^{3+} + H_2O_2$
10	$R_f - CF_2 - COOH + HO\bullet \rightarrow R_f - CF_2\bullet + CO_2 + H_2O$
11	$R_f - CF_2\bullet + HO\bullet \rightarrow R_f - CF_2OH \rightarrow R_f - COF + HF$
12	$R_f - COF + H_2O \rightarrow R_f - COOH + HF$

3.1.2. Impact of cycle hydration/dehydration

Water plays a fundamental role not only in facilitating proton conduction but also in maintaining the structural morphology and chemical integrity of PEMs. At the nanoscale, PEMs consist of a hydrophobic polymer backbone and hydrophilic side chains that carry functional groups, as mentioned before, forming phase-separated domains capable of solvating protons [68]. This nanophase separation, stabilized by hydrogen bonding and entropic forces, provides a percolated network for ion and solvent transport, as comprehensively discussed by Kusoglu and Weber [69]. However, the state of membrane hydration significantly influences both the physicochemical properties and the degradation pathways of PEMs. Under dry conditions (low relative humidity or elevated temperature), the contraction of hydrophilic domains

reduces proton mobility, lowers the ionization of sulfonic groups, and increases the membrane's internal resistance. Experimental and modeling studies by Kreuer [70] have shown that inadequate hydration disrupts the electrostatic environment required for effective proton transport, while also inducing local mechanical stress. Conversely, overhydration can cause excessive membrane swelling [71,72], leading to disruption of the optimal arrangement of proton-conducting channels, and in severe cases, water accumulation blocks gas diffusion paths at the electrode. Importantly, hydration status also governs the dominant chemical degradation mechanisms. Chen et al. [49] identified two distinct pathways associated with different relative humidity (RH) regimes: (i) main-chain unzipping under high humidity, and (ii) side-chain scission under dry conditions. At high RH, reactive end groups such as carboxylic acids (-COOH) initiate chain-unzipping reactions along the polymer backbone, resulting in the release of HF and small fluorinated fragments. Although the membrane thins progressively, some proton-conducting sites are retained. In contrast, under low RH, hydroxyl radicals (•OH) preferentially attack ether linkages (–C–O–C–) in the side chains, leading to the formation of trifluoroacetic acid (TFA) and the loss of sulfonic acid groups (-SO_3H), severely compromising proton conductivity and mechanical stability.

Recently studies have provided direct evidence of pinhole formation and crack propagation under fluctuating RH conditions, highlighting the synergetic effects of cyclic hydration-induced chemical and mechanical stress. These initial micro-defects can evolve over time into severe structural failure, impairing gas separation and ultimately reducing the overall fuel cell lifetime [73–77].

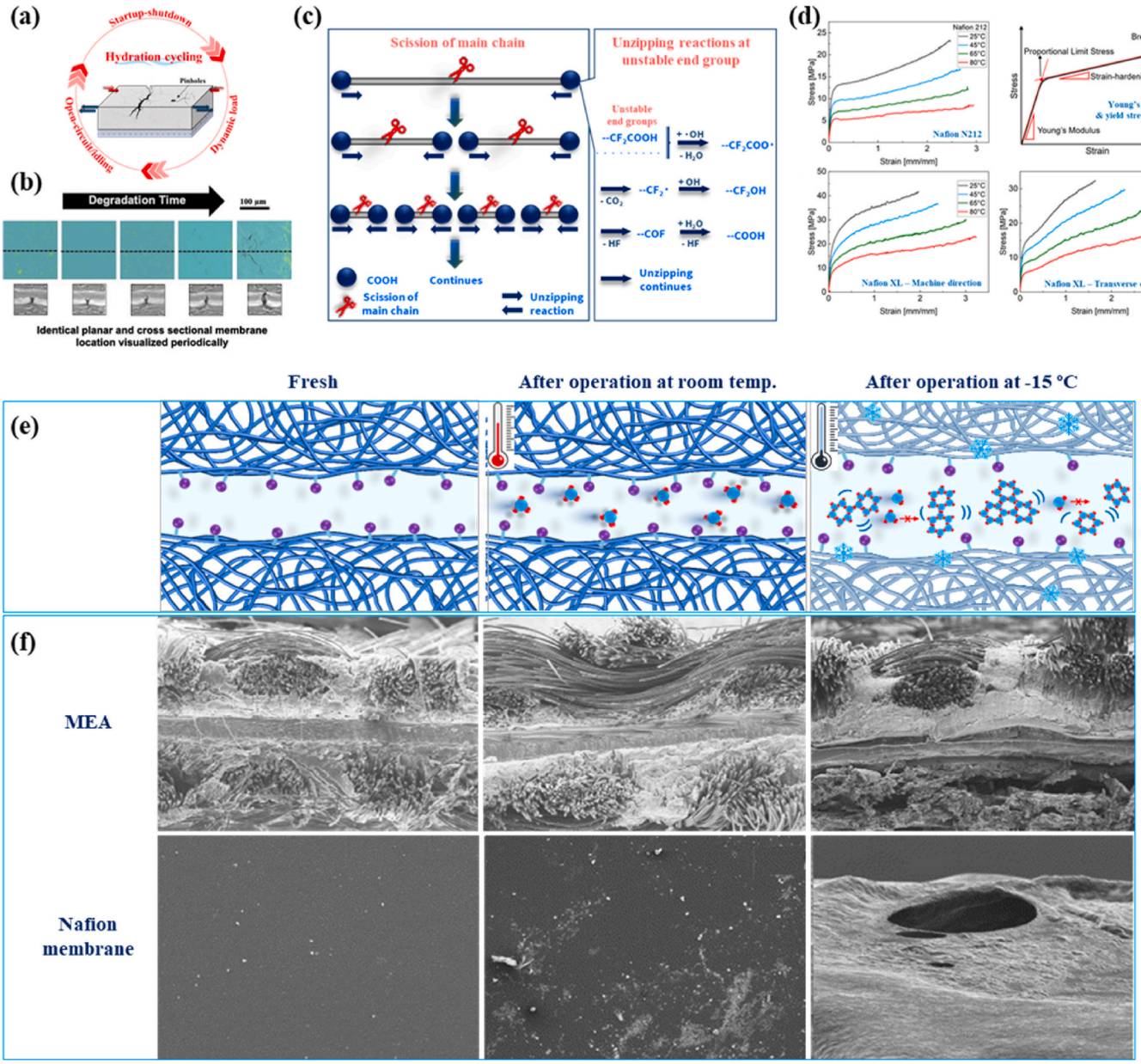

Fig. 4. (a) Cyclic hydration-induced stress in PEMs and the generation of tensile strain across the membrane-electrode interface. (b) Cyclic swelling data for composite reinforced membranes under hydration/dehydration cycles (adapted from Ramani et al. [82]). (c) Thermal degradation mechanisms in PEMs: main-chain scission, unzipping reactions at unstable polymer ends, and carboxylic acid groups formation, leading to thinning and instability. (d) Stress-strain behavior of Nafion® membranes at different temperatures. Nafion 212 shows reduced stiffness, Young's modulus, and yield stress with rising temperature; Nafion XL, with ePTFE reinforcement, has higher values but greater thermal sensitivity (adapted from Shi [83]). (e) Effect of sub-zero temperature on MEA and PEM: frozen water disrupts H-bonds, blocks proton channels, and induces stress. (f) SEM images of mechanical deformation and microcracking (adapted from Yan et al. [84]).

3.2. Mechanical degradation by cyclic swelling fatigue and crack propagation

Among various failure modes affecting PEMs, mechanical degradation is particularly significantly in thinner membrane, which although beneficial for reducing Ohmic losses, but tend to be more vulnerable under mechanical and environmental stresses. Consequently, optimal membrane design must strike a balance between conductivity and mechanical integrity. Unlike chemical degradation, which originates from bond cleavage and oxidative damage, mechanical degradation is primarily physical. It results from a combination of operational stresses (pressure differentials, hydration cycles) and material vulnerabilities (low tensile stress, thin structure). The consequences range from membrane thinning and microcracks to delamination, blistering, and pinhole formation, all of which directly undermine the cell's lifetime and gas barrier properties. Two major factors govern this degradation pathway: Operating conditions and intrinsic material properties.

Under the first category, numerous studies have shown that PEMs exposed to fluctuating open-circuit voltages, temperature cycling, and especially repetitive changes in RH exhibit significantly accelerated degradation rates [37,56,78]. Such variations lead to mechanical fatigue and internal stress buildup across the membrane thickness. For the second category, the mechanical robustness and flexibility of the membrane material itself are crucial. Stiffer or chemically aged membranes fail to accommodate mechanical distortion, leading to crack propagation under cyclic strain [79]. Repeated hydration and drying cycles cause the membrane to expand and contract unevenly, especially near the electrode interface, where it is subjected to the greatest mechanical constraint. Over time, this repetitive stress drives fatigue accumulation and leads to the formation of microcracks [56,80] (Fig. 4a). For instance, Lai et al. [81] reported up to a 15 % increase in membrane thickness during hydration and a 4 % shrinkage during dehydration. Ramani et al. [82] observed swelling as high as 30 % in the through-plane direction in reinforced ePTFE composite membranes (Fig. 4b).

In comparison, thermal cycling is generally considered less damaging than RH cycling, though it can still contribute to localized stress under certain conditions. The accumulated stress leads to mechanical fatigue, which causes defects to propagate through the membrane as interfacial cracks and eventually transitions into pinhole defects. Fatigue testing has shown that crack networks resembling "mud-cracks" form in the electrode layers and gradually evolve into perforation and gas crossover after 500–600 h of cycling [85]. In addition to hydration-induced fatigue and membrane swelling, localized mechanical stress due to manufacturing imperfections and operational asymmetries can further exacerbate membrane damage. Surface roughness in the gas diffusion layer, residual particulates, uneven clamping force, and inactive membrane zones create in-plane stress gradients that concentrate at corners or edges of the MEA geometry [86]. These localized stresses act as nucleation sites for crack formation, particularly in areas that are already mechanically or chemically compromised. As mentioned before, chemical degradation directly weakens the membrane's ability to withstand mechanical stress. Chain scission during oxidative degradation reduces the molecular weight of the polymer and disrupts its viscoelastic properties, making the membrane more brittle. This renders the structure highly susceptible to even moderate RH cycling or pressure variations [80,86,87]. Ultimately, mechanical degradation is not an isolated pathway but interacts synergistically with chemical and thermal stressors, amplifying the likelihood and severity of pinhole formation. Recognizing this interplay is crucial for designing PEMs that remain robust under realistic loading conditions, without impacting proton conductivity.

3.3. Thermal degradation

Unlike chemical or mechanical degradation, which directly compromise the membrane's chemical or structural integrity, thermal degradation typically functions as an accelerant, intensifying other failure modes through its influence on water retention, polymer stability, and mechanical resilience. Temperature affects nearly every aspect of PEM behavior. Although PEMFCs are designed to operate within a moderate temperature range (60–80 °C), deviations above or below this window can destabilize the membrane physically and chemically. These stressors often act in conjunction with other degradation mechanisms, amplifying damage and ultimately leading to irreversible defects including pinholes. Among commercial PEMs, Nafion®, a widely adopted PFSA membrane, is noted for its high proton conductivity under hydrated conditions. However, this property depends mostly on the integrity of its phase-separated morphology and the continuity of water channels. At elevated temperatures, these features become compromised, while at sub-zero conditions, water freezing imposes internal mechanical stress. As such, thermal degradation does not typically initiate failure alone but critically lowers the threshold for mechanical fracture and chemical attack.

3.3.1. High-temperature dehydration and instability

Dehydration is a primary initiating factor in high-temperature membrane degradation. Water loss disrupts the hydrogen-bond network essential for proton transport and simultaneously weakens the structural stability of sulfonic acid side chains (–SO_3H) [88]. In the absence of sufficient water, the chemical structure becomes vulnerable to thermally driven chain scission reactions, especially near sulfonic groups and ether linkages. Bond cleavage of C–S or C–O–C moieties produces chemically reactive species such as SO_2, •OH, and perfluorinated fragments [10,89]. These degradation products act in a cascading reaction: once generated, radicals trigger further breakdown along the polymer backbone, weakening the mechanical resilience of the membrane and contributing to localized thinning [53]. As shown in Fig. 4c, this cascade includes side-chain detachment, unzipping reactions at polymer end groups, and the formation of carboxylic acid groups. Importantly, although the degradation may initiate at a molecular level, the physical consequence, emerges when the structural integrity is sufficiently undermined, and mechanical loading (from pressure differentials or membrane swelling) exceeds local strength thresholds [90]. Thermal exposure also has a pronounced effect on the bulk mechanical properties of PEMs. Fig. 4d reveals that the Young's modulus and yield stress of both Nafion® 212 and Nafion® XL decrease steadily from 25 °C to 80 °C, with Nafion® XL consistently showing higher absolute values due to its ePTFE reinforcement layer. However, the relative reduction with temperature is more pronounced for Nafion® XL, indicating higher thermal sensitivity [83]. The proportional limit stress and strain-hardening modulus also decline, while break strain increases, reflecting a shift toward greater ductility and reduced stiffness. Under high thermal loads, the membrane becomes more compliant and susceptible to deformation, facilitating local strain accumulation and crack initiation under operational stresses. This deterioration in mechanical integrity at elevated temperatures predisposes the membrane to thinning, tearing, and eventual pinhole formation during long-term operation.

In addition to molecular instability, thermal cycling introduces mechanical consequences through cyclic expansion and contraction of the membrane. These thermomechanical deformations, driven by changes in temperature and humidity, generate repeated tensile and compressive stress, particularly at mechanically vulnerable interfacial zones. Over time, these stresses contribute to material fatigue, interfacial delamination, and crack formation, serving as precursors to through-thickness defects including pinholes. Wu et al. [91] demonstrated that repeated dry-wet cycles applied to Nafion membranes over 300 h resulted in a near threefold increase in hydrogen crossover and a significant drop in open-circuit voltage.

3.3.2. Sub-zero operation and freeze-thaw damage

Thermal degradation is not limited to high temperatures. At sub-zero conditions, water trapped within the polymer matrix or interfacial regions freezes, expands, and imposes internal stress. This process disrupts the hydrogen-bonding network, impairs proton transport, and physically deforms the membrane structure. Experimental work by Yan et al. [84] also suggests that freeze-induced delamination can lead to mechanical failures in the membrane (particularly at the PEM and catalyst layer interface), especially near the edges of MEA regions with uneven hydration. While sub-zero-induced degradation does not follow a radical-based mechanism, it shares a common outcome: mechanical weakening that predisposes the membrane to perforation and pinhole formation (Fig. 4e and f).

3.3.3. Thermal degradation from localized heating

In addition to system-wide temperature excursions, localized thermal hotspots are often-overlooked source of degradation. These microdomains caused by uneven current distribution, inadequate cooling, or gas starvation, can reach temperatures several degrees higher than surrounding regions. Although these increases may seem minor, they are sufficient to trigger localized radical formation and chain scission events. More critically, once even a microscopic pinhole initiates, reverse hydrogen crossover reactions may occur at the cathode, generating further heat locally and creating a feedback loop of degradation. As a result, a hotspot may not only precede a pinhole but also drive its expansion once formed. Thus, hotspots function as nucleation zones where chemical, thermal, and mechanical degradation converge. Their presence helps explain why pinholes often appear not uniformly but at specific, sites of stress concentration near the inlet region or areas with water imbalance.

3.4. Synergistic effects of degradation modes

In practical PEMFC operation, membrane degradation does not proceed through a single, isolated mechanism. Instead, chemical, mechanical, and thermal stressors interact in complex, mutually reinforcing ways that accelerate the decline of membrane integrity. While Sections 3.1 to 3.3 detailed these degradation modes individually, their most destructive potential emerges when they converge, producing local environments where stress accumulates, exceeding the capacity of intrinsic repair mechanisms, and where structural failure becomes inevitable. Among the most serious outcomes of this convergence is the formation of pinholes, which often signify the final stage of membrane deterioration. The degradation sequence often begins with subtle chemical attack, notably by hydroxyl radical •OH generated near the catalyst layers [92]. These radicals degrade the sulfonated side chains and cleave vulnerable bonds in the polymer backbone, reducing the molecular weight and mechanical resilience of the membrane [25]. Even before visible damage occurs, this chemical weakening renders the material more brittle and less capable of absorbing stress [37]. At the same time, cyclic humidity fluctuations introduce repetitive swelling and shrinking of the membrane, particularly near interfaces, leading to fatigue stress and microcrack formation [93,94]. Areas already chemically compromised are less able to withstand these dimensional changes, and thus more likely to accumulate microdefects [25].

When the membrane is exposed to elevated temperatures, caused by high current density or insufficient cooling, it gradually loses mechanical strength, as shown in Fig. 4d. At the same time, dehydration reduces proton conductivity and promotes the formation of radicals [95]. These two effects often overlap in localized regions, particularly near interfaces, where heat and stress accumulate [37,96]. Under such conditions, early-stage microcracks, formed by humidity cycling or chemical weakening, may grow and connect, eventually cutting through the membrane and forming pinholes (Fig. 5) [95,97].

Notably, these processes do not occur uniformly across the membrane surface. Regions near the catalyst-membrane interface, the inlet edges, or areas of uneven hydration are especially vulnerable. Advanced diagnostic studies, including focused ion beam-scanning electron microscopy (FIB-SEM) and *in situ* tomography, have revealed that many pinholes originate in these zones where multiple stressors intersect [98,99]. The co-location of gas crossover, metal contaminants, and pressure gradients makes these regions particularly susceptible to early-stage failure evolution.

Importantly, this convergence of degradation mechanisms poses a significant challenge for prediction and control. While each individual mechanism may be well-characterized, their interactions are inherently nonlinear and site-specific. Modeling studies have attempted to map these coupled effects, but few provide comprehensive frameworks that account for the dynamic interplay between chemical breakdown, mechanical fatigue, and thermal softening under real-world conditions [17,20,100–102]. Recent modeling efforts have also begun to quantify the synergistic effects among degradation pathways. Placca and Kouta [36] employed a Fault Tree Analysis model to probabilistically map the interdependence between chemical, mechanical, and thermal degradation processes in PEMFCs. Their results indicated that mechanical degradation events, particularly pinhole formation, represent the dominant failure mode, with a simulated probability of approximately 7×10^{-5} after 1000 simulations of 100 h of operation in cycling conditions. Complementarily, Peng et al. [103] developed a simulated-annealing-inspired infrared diagnostic model that quantitatively correlated thermal response parameters with actual pinhole size, achieving a strong exponential fit ($R^2 > 0.97$). Together, these studies provide both system-level and phenomenon-level perspectives on how stress coupling quantitatively accelerates pinhole initiation, offering a foundation for predictive lifetime modeling and defect-informed diagnostics in PEM membranes. This complexity underscores the critical need for integrated material strategies and multi-modal diagnostics that can detect and suppress emerging defects before they evolve into pinholes. Developing kinetic or probabilistic frameworks capable of linking radical concentration, stress amplitude, and temperature to measurable degradation rates would be a key step toward predictive lifetime modeling and durability optimization in PEMFC membranes.

3.5. Pinhole characteristics and their impact on performance and safety

The functional impact of pinholes on PEMFC performance is profound and multifaceted. Even a single microscopic pinhole can fundamentally undermine the membrane's role as a selective ionic conductor and gas barrier, allowing direct hydrogen and oxygen crossover. Operationally, an increase in hydrogen crossover together with OCV decay is consistent with pinhole nucleation and early growth under the DOE accelerated stress test conditions [29]. This crossover not only reduces fuel utilization efficiency but also creates localized sites for undesired chemical reactions, which can lead to the generation of ROS and the onset of further chemical degradation [104,105]. In particular, the exothermic nature of H_2/O_2 recombination at the pinhole site can produce localized heating, with temperatures reported to exceed 140 °C, far above the glass transition temperature of Nafion [28,106]. Thereby increasing the risk of polymer softening, catalyst particle aggregation, and mechanical destabilization of the MEA. These local changes can propagate rapidly, as the feedback between gas crossover, heat generation, and chemical attack accelerates both the growth of the initial defect and the emergence of secondary degradation processes [107,108]. Table 3 below summarizes the key functional impacts of pinhole formation and their associated mechanisms.

These outcomes are not limited to isolated degradation but often trigger cascading effects. Pinhole-driven gas crossover promotes ROS generation, which in turn accelerates chemical attack on surrounding membrane regions [23]. Localized heating softens the membrane, increasing susceptibility to mechanical fatigue. In full-scale stacks, even a single pinhole can create cell-to-cell voltage imbalance [25,114], increase hydrogen losses, and damage auxiliary components like valves or

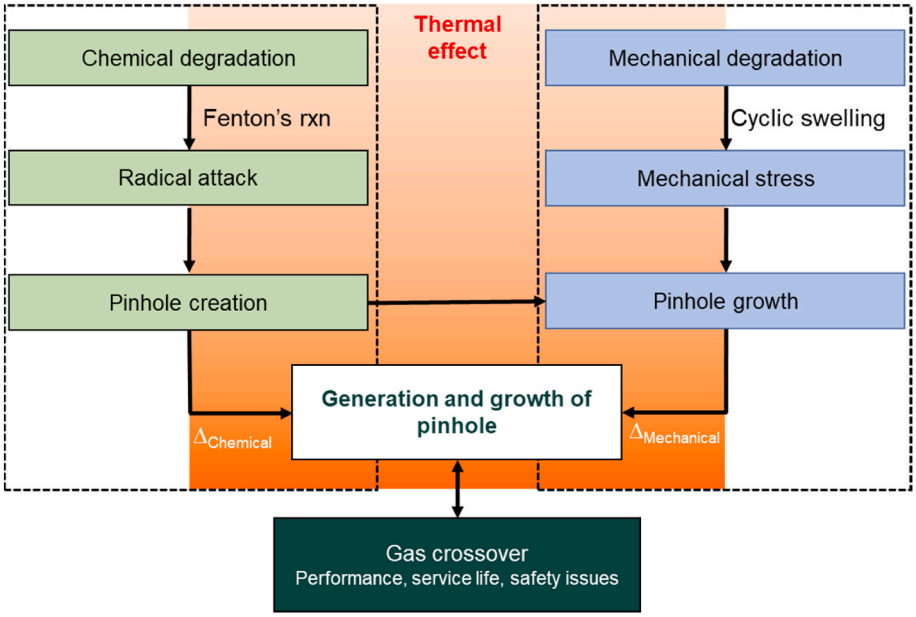

Fig. 5. Flowchart illustrating the synergistic contributions of chemical, mechanical, and thermal degradation pathways leading to pinhole formation in PEMs.

Table 3
Summary of major functional impacts resulting from pinhole formation in PEMFCs.

Type of impact	Underlying mechanism	Degradation factors	Consequences on PEMFC	Ref.
Gas crossover	Direct permeation of H_2 and O_2 through pinhole defects	Physical leakage through pinhole	Efficiency loss, local hot spots, ROS generation	[25]
Chemical degradation	Radical-induced attack accelerates polymer chain scission	•OH, (hydrogen peroxide) H_2O_2 generation at defect sites	Loss of ionic conductivity, membrane thinning, fluoride emission	[37,79]
Mechanical failure	Local stress accumulation and layer delamination	Hydration cycling, local strain	Crack propagation, mechanical rupture	[20,95]
Electrical distortion	Local current distortion due to non-uniform conductivity	Hotspots and ohmic losses	Reduced voltage output, non-uniform power distribution	[109–111]
Safety risks	Risk of explosion due to gas accumulation in crossover zone	$H_2 + O_2$ mixture in defect region	Operational hazard, system shutdown, possibility of local combustion	[112,113]

humidifiers due to sustained crossover and involved reactions [113, 115]. Under pressurized condition, explosive gas mixing becomes a serious safety concern. In practical fuel cell systems, pinhole defects rarely remain isolated. Once initiated, they propagate rapidly, particularly under high current density and startup-shutdown cycles. This makes early detection difficult, as voltage decay is often sudden and localized. The insidious nature of these defects means that by the time a pinhole is detected, system-wide performance may already be compromised [23,30,114].

Taken together, pinholes represent more than just morphological signs of degradation, they are functional tipping points where mechanical, thermal, and chemical stressors converge. Their small size belies their critical impact on fuel cell reliability, safety, and commercial viability, making their prevention and early detection a top priority in modern PEMFC design.

4. Detection and diagnostic techniques

Pinhole formation represents a critical turning point in the degradation of proton exchange membranes, serving not only as a structural defect but also as a functional failure that undermines membrane selectivity, promotes gas crossover, and accelerates further degradation. Given their small size and often hidden nature, pinholes may remain undetected until their consequences become severe. Therefore, reliable and timely detection methods are essential, not only for post-mortem failure analysis but more importantly for *in situ* monitoring and preventive diagnostics. To address this need, a range of diagnostic techniques has been developed to identify pinholes and assess their impact on membrane integrity and overall fuel cell performance. To provide a systematic overview, this section classifies diagnostic strategies into three primary categories based on their functional principles: (1) imaging-based localization techniques, (2) electrochemical detection techniques, and (3) gas leak testing techniques.

4.1. Imaging-based localization techniques

These techniques aim to spatially identify membrane defects by capturing thermographic, electrical, or morphological deviations. They are particularly valuable when the localization of damage is required for further analysis or targeted intervention.

Optical microscopy (OM) and scanning electron microscopy (SEM) are among the most commonly used techniques for visual inspection of membranes before and after operation. SEM offers high-resolution structural insights into the shape, size, and morphology of defects, while OM provides a broader surface overview [116]. Nevertheless, both are *ex situ* techniques, requiring sample preparation and limiting their use in real-time diagnostics.

Infrared thermography (IRT) is a non-destructive technique that detects thermal hotspots on the MEA surface using infrared cameras. These hotspots arise from localized exothermic recombination of hydrogen and oxygen at pinhole sites [117]. IRT enables non-invasive, real-time localization of pinholes, particularly under load cycling or steady-state conditions. Typical detection thresholds range from 10 to 100 μm [23]. Limitations include dependence on cell architecture, electrode

aging, thermal properties of adjacent layers, and sensitivity to thermal and electrical operating conditions. Recent studies [103,118–120] employing infrared reactive-flow-through imaging demonstrated that pinholes and electrode defects generate localized hotspots that can be rapidly identified on the MEA surface. By combining infrared (IR) imaging and OM collected after membrane aging tests, Chandesris et al. [116] visually identified the formation of a pinhole in the upper-right region of the MEA surface (Fig. 6a). When observed under optical microscopy, the same location revealed a perforation, confirming the accuracy of IR-based localization. This cross-validation demonstrates the effectiveness of combining imaging techniques for defect mapping.

4.2. Electrochemical detection techniques

Electrochemical techniques offer practical and non-invasive tools for monitoring membrane health in PEM fuel cells, particularly in identifying pinhole formation during operation. As pinholes evolve, they alter electrochemical behavior in characteristic ways, making them detectable through variations in current, voltage, and impedance. The following methods are commonly used for this purpose:

Hydrogen crossover current measurement: This technique directly quantifies the diffusion of hydrogen from the anode to the cathode across the membrane [124]. Under ideal conditions, protons selectively cross the membrane while hydrogen and oxygen remain isolated. However, when pinholes form, hydrogen permeates and gets oxidized at the cathode, generating a measurable current even at open-circuit conditions [125,126]. This crossover current increases as the membrane degrades, making it a sensitive parameter for *in situ* diagnosis [121]. Hydrogen crossover can be assessed via LSV, in which the working electrode (typically the cathode) is swept linearly in potential in a hydrogen/nitrogen configuration. Any crossover hydrogen is oxidized at the cathode, generating a measurable current that reflects the extent of gas permeation through the membrane and serves as a proxy for defect severity [127]. LSV provides a dynamic and voltage-resolved picture of hydrogen crossover behavior, which is particularly useful for comparing membranes or testing under variable hydration conditions [128]. According to DOE durability protocols, hydrogen crossover currents exceeding ~15 mA cm^{-2} in LSV-based measurements are regarded as a failure threshold, providing a quantitative benchmark for assessing membrane integrity [29]. Gunji et al. [129] showed that pinholes often formed in regions exhibiting high crossover currents and insufficient thermal dissipation. Their findings suggest that hydrogen crossover not only signals structural damage but also contributes to localized heating, which exacerbates thermal degradation. In a complementary study, Kreitmeier et al. [28] employed thermochromic pigment mapping and detected localized membrane temperatures exceeding 140 °C around pinhole sites, well above the glass transition temperature of most PFSA membranes. These thermal deviations were accompanied by evidence of polymer melting, providing direct proof that hydrogen crossover induces thermal stress sufficient to compromise membrane integrity. While hydrogen crossover measurement is highly sensitive and quantifiable, its diagnostic resolution is limited when used in isolation. Specifically, the technique cannot easily distinguish between uniform membrane thinning and localized perforations such as pinholes unless

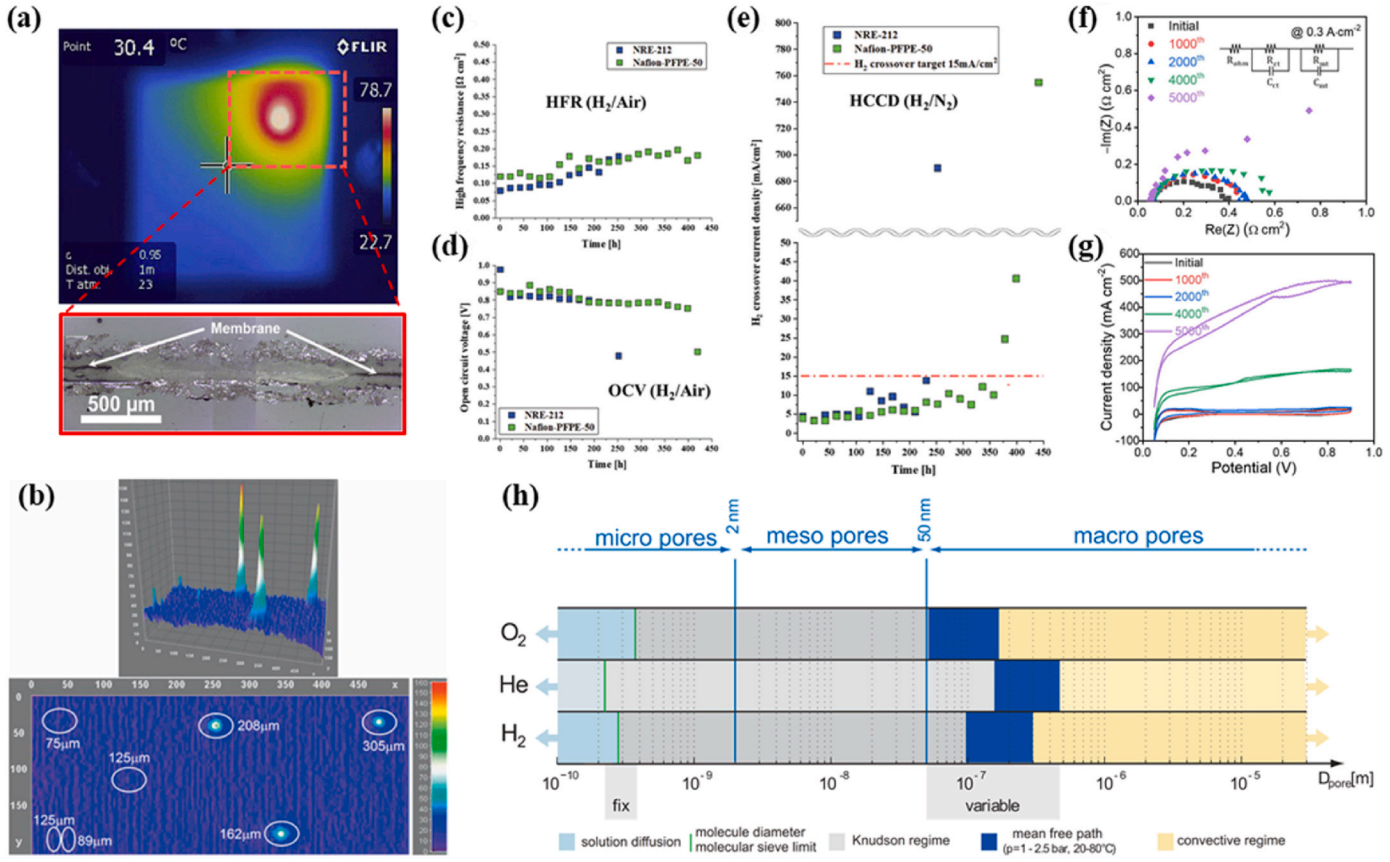

Fig. 6. (a) Localization of pinhole using combined IR and OM analysis (adapted from Chandesris et al. [116]). (b) Infrared thermography calibration based on pinhole size, highlighting the sensitivity of IR detection for early-stage defects (adapted from De Moor et al. [117]). Electrochemical performance variations of a PEM membrane under wet/dry accelerated stress testing: (c) Evolution of HFR, (d) open circuit voltage (OCV), and (e) hydrogen crossover current density over time, as monitored using DOE evaluation protocols (adapted from Kim et al. [121]). Additional electrochemical diagnostic tools used for periodic assessment include: (f) Nyquist plots from electrochemical impedance spectroscopy (EIS), and (g) cyclic voltammetry (CV) curves (adapted from Choi et al. [122]). (h) Schematic illustration of molecular diffusion, Knudsen diffusion, and viscous flow mechanisms across degraded PEM layers and pinhole sites (adapted from Kreitmeier et al. [123]).

coupled with spatially resolved imaging tools. Moreover, LSV measurements require stable test configurations and are typically conducted in specially designed fuel cell test cells or hydrogen pumps, which limits their routine applicability in full-stack systems. Despite these limitations, crossover current monitoring remains a cornerstone for *in situ* assessment of PEM degradation, particularly when integrated into multi-modal diagnostic frameworks.

Open circuit voltage (OCV): Under ideal conditions, the OCV of a PEMFC reflects the thermodynamic potential difference between the hydrogen and oxygen electrodes. However, the presence of pinholes causes hydrogen and oxygen to mix and react internally, leading to parasitic reactions that lower output cell voltage. A sharp or progressive drop in OCV, especially during shutdown or startup conditions, may indicate gas crossover caused by microstructural defects, including pinholes [130–132]. DOE criteria set a relative OCV loss of $\geq$20 % under specified conditions as a practical threshold of membrane failure, providing a useful reference for durability evaluation [29]. Nonetheless, OCV degradation is not exclusively indicative of pinhole formation. Other phenomena such as catalyst degradation, membrane thinning, and contamination may also contribute to voltage decay [37,122,133]. Therefore, OCV monitoring is more effective as a preliminary indicator, best interpreted in combination with crossover current data or imaging diagnostics for confirmatory analysis.

Cyclic voltammetry (CV) though not a direct diagnostic tool for pinholes, can provide complementary insights into catalyst layer degradation and potential local fuel starvation, both of which can be consequences of membrane damage [134]. When pinholes form, gas crossover can shift the local electrochemical environment, altering double-layer capacitance and pseudocapacitive features observable in CV curves. Deviations from expected voltammetric profiles may indicate disturbed gas distribution or increased parasitic reactions within the MEA [122].

Electrochemical impedance spectroscopy (EIS) is widely used to characterize membrane and cell impedance in both frequency and time [135]. By analyzing Nyquist plots, changes in membrane resistance, charge transfer resistance, and mass transport resistance can be tracked over time [127]. As pinholes form and expand, these parameters deviate significantly from their baseline values, reflecting the loss of membrane integrity and ionic conductivity [122]. EIS is particularly powerful when used periodically during long-term tests [24], as changes in impedance spectra can precede visible physical failure, offering a predictive advantage. When integrated with crossover current or thermal imaging, impedance analysis strengthens the reliability of pinhole diagnostics. Fig. 6c–g summarizes representative examples of the measurements described above.

Cell voltage decay monitoring under during startup, shutdown, or under accelerated stress conditions is a straightforward but informative technique. During normal operation, voltage should remain relatively stable for a given current density. However, the appearance of pinholes introduces gas leakage and uncontrolled side reactions, which disrupt the electrochemical balance and cause localized or system-wide voltage decay. A rapid voltage drop during constant current operation, or unstable voltage behavior during OCV, may indicate the presence of growing defects [117]. Although voltage decay is a non-specific signal, it remains a practical and scalable method for online monitoring, particularly in automotive or distributed PEMFC systems, where complexity and instrumentation may be limited.

4.3. Gas leak testing techniques

The presence of pinholes in PEMs alters the gas transport mechanisms through the membrane, which provides a basis for diagnostic techniques based on gas crossover and electrochemical signals. Gas can permeate through the membrane via three primary mechanisms: molecular diffusion, Knudsen diffusion (through nanometer-sized pores), and viscous flow (through micrometer-scale pinholes), as illustrated in Fig. 6h [123]. While molecular and Knudsen diffusion are driven by partial pressure differences, viscous flow through pinholes responds to total pressure differentials. This distinction allows one to differentiate between uniform membrane thinning and localized pinhole formation. By controlling pressure gradients across the membrane, the dominant transport mode can be isolated to assess the severity and nature of membrane degradation. Several gas leak testing techniques have been developed to exploit these phenomena:

Pressure drop testing [136,137] tracks the pressure decay between the anode and cathode compartments to identify major leaks, making it suitable for full-system screening. This method is simple and inexpensive and proves effective for identifying significant leaks or punctures. However, it lacks the sensitivity needed to detect early-stage or microscopy pinholes.

For higher sensitivity, *helium leak detection* [136,138] is often employed. This technique introduces helium gas, selected for its low molecular weight and inert nature, into one chamber of the cell. The emergence of helium on the opposite side is then measured using a mass spectrometer. Due to helium's small atomic size and high diffusivity, this method is capable of detecting micro-defects at extremely low concentrations, making it suitable for *ex situ* quality control during membrane manufacturing. Nevertheless, the requirement for specialized instrumentation limits its *in situ* applicability.

For quick and direct visual confirmation of gas leakage, *the bubble test (or gas leakage visualization)* is frequently used [123,136,139]. In this method, a soapy solution is applied to the suspected area, and the formation of bubbles reveals gas escape. While highly accessible and useful for pinpointing the location of major leaks, the test is qualitative in nature and unsuitable for small or early-stage defects. In practice, the effectiveness of these gas leak testing techniques can be influenced by spatial variations in temperature, humidity, and pressure throughout the fuel cell. For this reason, gas-based methods are often combined with imaging or electrochemical diagnostics to improve spatial resolution and enhance overall reliability.

Taken together, gas leak testing techniques form a critical component of the diagnostic method for PEMFCs, offering complementary insights to electrochemical and imaging approaches, particularly when used in hybrid strategies aimed at early detection and prevention of catastrophic pinhole-driven failures.

4.4. Summary and comparative assessment of pinhole diagnostic techniques

Pinhole formation in PEMs represents a critical degradation event that undermines both structural integrity and electrochemical performance. As shown in the previous sections, these defects rarely occur in isolation, but often the result of complex and interacting chemical, mechanical, and thermal stressors. To effectively monitor and understand this failure mode, a multi-pronged diagnostic approach is essential. Each method offers unique insights into the onset, localization, and impact of pinholes, but none is fully sufficient when used alone.

Advanced imaging techniques, particularly infrared thermography and electron microscopy, have enabled researchers to visualize the physical manifestation of pinholes and track their progression over time. For instance, *in situ* infrared analysis has been used to detect localized thermal deviations on the MEA surface, often precursors to pinhole formation [103,117], while post-mortem SEM has revealed characteristic crater-like structures ranging from a few micrometers to over 100 μm in size [25], particularly concentrated near gas inlet and outlet zones where humidity and stress gradients are high. These observations underscore the spatial dependence of pinhole initiation, typically near mechanically or chemically vulnerable regions.

Electrochemical diagnostics further this understanding by capturing real-time functional changes associated with membrane defects. Voltage decay at constant current and OCV drops are frequently reported as early indicators of hydrogen crossover, which often accompanies or

precedes pinhole formation [48,51,114]. Techniques such as LSV and EIS can quantify crossover currents and monitor changes in proton conductivity, respectively, both of which are affected as defects enlarge [140,141]. Moreover, segmented cell studies have allowed spatial mapping of current distribution and impedance, revealing the localized impact of pinholes on electrochemical behavior [28].

Gas-based techniques complement these methods by focusing on transport phenomena. Pressure decay and helium leak testing offer high sensitivity in *ex situ* screening, while gas composition analysis during cell operation provides indirect confirmation of crossover. As shown in Fig. 6h, the transport regime, whether molecular diffusion, Knudsen diffusion, or viscous flow, can help distinguish between uniform membrane thinning and structural perforation. These methods are particularly effective when aligned with theoretical models and crossover simulations [50], which help decouple physical gas leakage from electrochemical interference.

Case studies from the literature reinforce the importance of integrated diagnostics. In a long-term durability study by Paredes et al. [142] showed that extended operation (up to 12,000 h) results in thinning of the catalyst layer and membrane, most notably near the cathode inlet. SEM and optical microscopy confirmed the emergence of pinholes and associated mechanical fatigue. To complement these observations, representative cross-sectional SEM images from a dynamic accelerated stress test are presented in Fig. 7a–b, highlighting that similar thinning and microstructural degradation can be reproduced under accelerated protocols [143]. In a similar approach, Taylor et al. [114] employed a combined chemical and mechanical accelerated stress test to probe degradation behavior. Fig. 7c indicates that the changes in OCV transients during AST cycles were used to track the onset of degradation, culminating in pinhole formation as the final failure event. This progression was further confirmed by post-mortem SEM and optical analysis conducted by Stanic and Hoberecht [25], who observed the emergence of actual pinholes in MEAs subjected to *in situ* durability testing under hydrogen and oxygen exposure. For reference, a representative SEM image of such pinholes (Fig. 7d) provides a direct visualization of their morphology in degraded MEAs [24].

However, the ability to systematically compare pinhole onset times across studies remains limited due to variations in test conditions, material properties, and evaluation methods. To address this, Qui et al. [101] categorized durability evaluation methods into *in situ* and *ex situ* protocols, where lifetime testing and AST were particularly effective in enabling real-time observation of defect evolution. Ultimately, the detection and characterization of pinholes in PEMs benefit most from a hybrid approach, one that combines spatially resolved imaging, real-time electrochemical analysis, and transport-based gas diagnostics. Table 4 presents a comparative summary of the key techniques, outlining their advantages, and limitations. This integrative strategy not only improves our ability to detect defects before failure occurs but also provides critical input for the rational design of pinhole-resistant membranes.

5. Strategies to prevent pinhole formation and propagation

Effectively mitigating the formation and propagation of pinholes requires solution rooted in material design. By optimizing membrane chemistry, architectural structure, and surface properties, ability to enhance resistance to mechanical stress, chemical attack, and defect propagation can be significantly. The following section organizes recent advances into three closely related innovations in polymer chemistry, composite architectures, and surface modification.

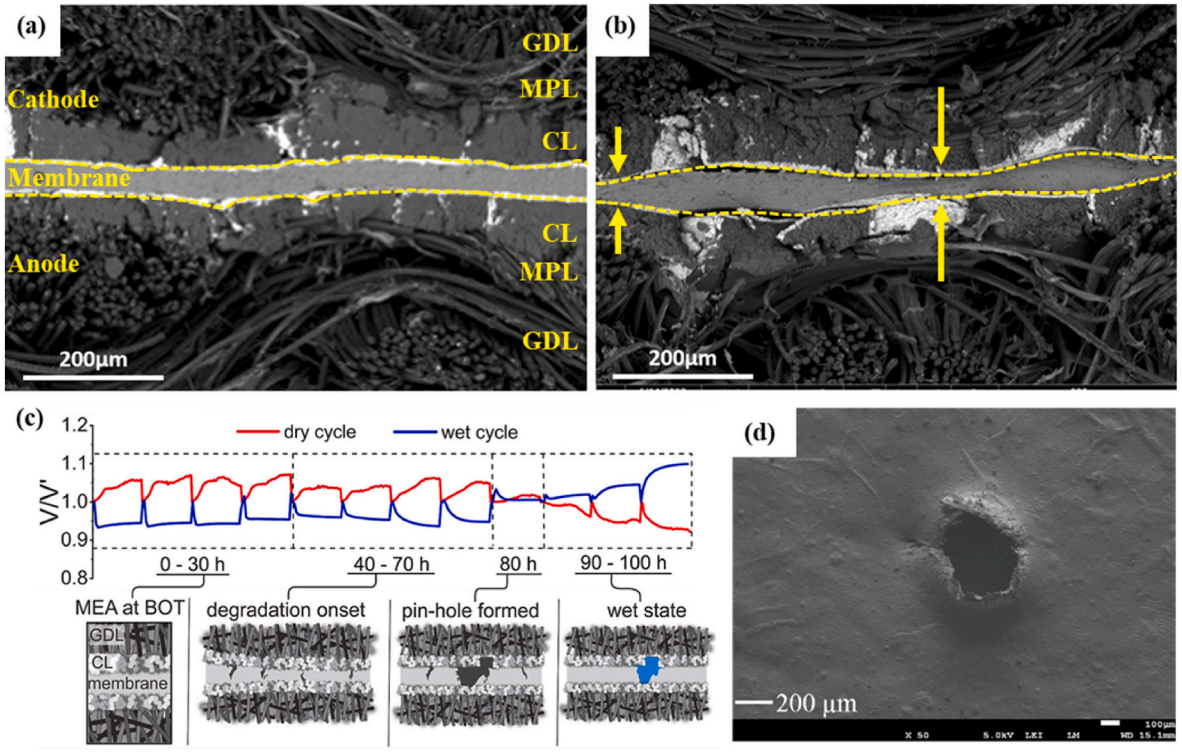

Fig. 7. Cross-sectional SEM images of the MEA before and after dynamic accelerated stress testing: (a) Pristine MEA and (b) MEA aged for 1000 h under the AST program. Aging leads to thinning/compaction of functional layers (microporous layer - MPL and CL), micro-crack initiation, and pore coalescence, indicating loss of mechanical integrity and increased susceptibility to local defects that can evolve into pinholes (adapted from Birkner et al. [143]). (c) Degradation progression of the membrane, as evidenced by changes in OCV transients during accelerated stress testing. From left to right (increasing test duration), the MEA initially shows stable behavior. A gradual drop in OCV after approximately 40 h indicates the onset of membrane degradation, which eventually leads to pinhole formation and rapid voltage decline (adapted from Taylor et al. [114]). (d) SEM image of pinholes in MEA (adapted from Huang [25]).

Table 4
Comparative overview of diagnostic techniques for pinhole detection.

Technique	Detection Limit	Localization	*In situ* Compatible	Advantages	Limitations	Ref.
Infrared thermography	30–100 μm	Yes	Yes	Real-time, localized detection	Sensitive to thermal/electrical conditions	[103,144, 145]
OM/SEM	~1 μm (post-mortem)	Yes	No	High-resolution structural information	Requires sample preparation	[25, 145–147]
Hydrogen crossover current	Indirect	No	Yes	Quantitative, adaptable to test benches	Dependent on humidity and catalyst aging	[29,121,148]
Helium gas detection	Indirect	Yes	No	High sensitivity, industry-standard	Requires costly instrumentation	[136,138]
Electrochemical impedance	Indirect	No	Yes	Multi-parameter insight	Needs modeling, not pinhole-specific	[29,121,148]
Voltage decay monitoring	Indirect	No	Yes	Easy to implement, real-time trends	Non-specific, may miss early damage	[29,117,148]
Bubble test	>100 μm	Yes	No	Visual confirmation	Destructive, qualitative only	[123,136, 139]

5.1. Polymer chemistry modifications

The two dominant chemical degradation pathways in PEMs, radical attack on hydrophilic side chains and backbone scission at ether linkages, originate from distinct but interconnected mechanisms [69,149]. Consequently, durable membrane design must integrate chemistries that synergistically enhance oxidation resistance (to mitigate radical attack) and mechanical robustness (to suppress crack initiation and propagation).

Short side-chain PFSA (SSC-PFSA): By shortening the $–OCF_2CF_2–SO_3^-$ side chains (Fig. 8a), SSC-PFSA membranes such as Aquivion®, represent a significant advancement over traditional long side-chain (LSC) analogues like Nafion™ due to their unique combination of high-water retention and mechanical robustness. This dual advantage arises from increased crystallinity in hydrophobic domains and reduced side-chain mobility, which together mitigate swelling-shirkage stress while maintaining high proton conductivity. Recent studies have demonstrated that SSC-PFSA membranes outperform their

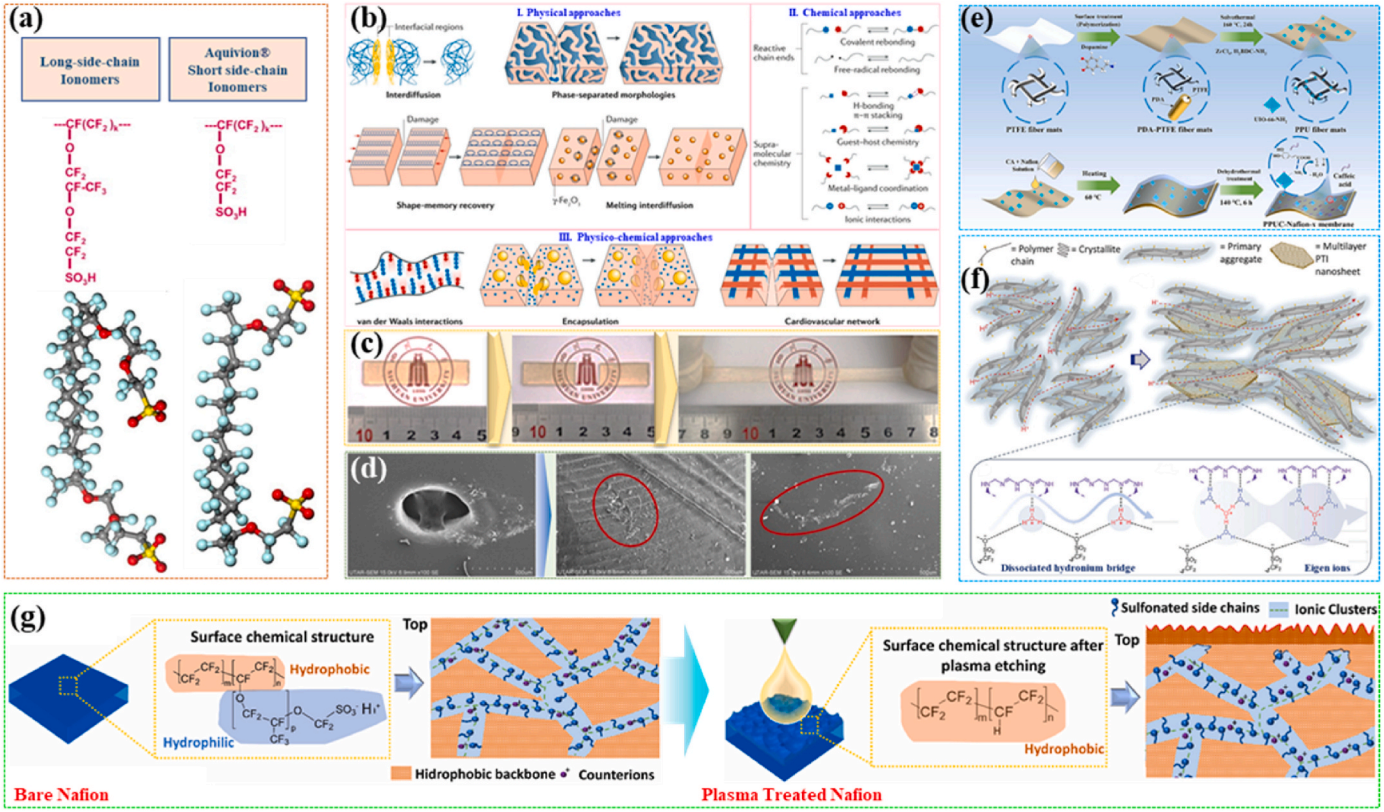

Fig. 8. (a) Polymer structure for long-side chain Nafion® and short-side chain Aquivion® perfluorosulfonic ionomer membranes (adapted from Stassi et al. [151]). (b) Schematic illustration of self-healing mechanisms in polymers, showing intrinsic and extrinsic approaches including reversible bonding and capsule/vascular-based healing (adapted from Wang et al. [152]). (c) Observable self-healing behavior of the polymer (adapted from Li et al. [153]). (d) SEM images comparing the damaged pristine membrane and the self-healed membrane (adapted from Wuen Ng et al. [154]). (e) MOF/PDA@PTFE fibrous mats prepared through in-situ MOF growth using a hydrothermal synthesis method (adapted from Liu et al. [32]). (f) Simplified membrane architecture of Nafion, progressing from left to right: PTI incorporation aligns and enlarges secondary ionomer aggregates while reducing crystallite size and spacing to enhance long-range proton transport. Acid-base interactions between sulfonate groups and PTI pyridinic nitrogen facilitate proton hopping: hydronium bridges are stabilized under dry conditions, while Eigen-like ions persist at low humidity (adapted from Smith et al. [155]). (g) Schematic illustration of how plasma etching alters the Nafion surface, resulting in the closure of surface ionomer channels (adapted from Barbosa et al. [156]).

LSC counterparts under a wide range of operating conditions. Cha et al. [150] demonstrated that Aquivion® membranes in self-humidifying PEMFCs delivered up to 15 % higher power density and exhibited superior stability under varying back pressure at high voltages, while also maintaining a faster dynamic response and shorter voltage-settling times at low voltages. Furthermore, high-temperature durability tests by Stassi et al. [151] revealed that SSC-PFSA membranes possess lower ohmic resistance, reduced gas crossover, and enhanced mechanical stability, attributed to their higher glass transition temperature and crystallinity, resulting in suppressed dry-out effects and delayed pinhole initiation. Collectively, these findings confirm that SSC-PFSA membranes not only improve water management and mechanical resilience but also extend pinhole-free operation and long-term durability under demanding PEMFC conditions, making them a benchmark for next-generation membrane materials.

Self-healing membrane: One of the emerging development directions in recent years is the design of polymer exchange membranes incorporating self-healing technology. This concept is inspired by the ability to restore broken bonds through polymer chain diffusion and the reformation of reversible hydrogen bonds at damaged sites [157–159]. To better illustrate how these concepts translate into practical designs, Fig. 8b first presents a generalized view of self-healing mechanism, which can be further examined in detail in the work of Wang et al. [152], followed by representative examples highlighting observable polymer recovery and structural integrity after damage (Fig. 8b–d). A representative example is the hybrid N/PVA/SGO membrane system, which demonstrates notable self-healing capability in terms of both methanol permeability and tensile strength after mechanical damage [154]. The self-healing mechanism is believed to originate from a combination of hierarchical hydrogen bonding interactions and adhesive forces between SGO and the polymer network, which enhance chain reconnection and help preserve the structural integrity of the membrane. Although full recovery has not yet been achieved, especially after repeated damage cycles, the promising preliminary results indicate that self-healing membranes represent a potential strategy to improve long-term durability and resistance to pinhole formation in PEMs. This is particularly relevant when using functional materials such as PVA and SGO, which offer dynamic molecular-level interactions conducive to healing behavior.

5.2. Composite and nanostructured membranes

Focusing on integrating inorganic nanomaterials, functional fillers, and multi-dimensional reinforcements into the polymer matrix, is also other ways to address the intrinsic weaknesses of PEM. The incorporation of expanded polytetrafluoroethylene (e-PTFE) as a reinforcing scaffold within PFSA matrices has been shown to significantly improve membrane mechanical properties and suppress defect propagation. Dong et al.'s study [160] demonstrated that polyphenolamine-treated e-PTFE, combined with ZrO_2 nanoparticles functionalized with redox-active surface groups, forms a three-dimensionally-reinforced hydrogen bonding network. This architecture not only enhances interfacial compatibility and proton conductivity (up to 0.203 S cm^{-1} at 80 °C), but also confers high tensile strength (50.7 MPa) and remarkable durability, with only 13.5 % mass loss after 72 h in Fenton's reagent and stable operation through 5500 dry/wet cycles. More recently, Liu et al. [32] reported a metal-organic framework (MOF)-decorated PTFE membrane immobilized with caffeic acid radical scavengers (Fig. 8e). This strategy stabilized antioxidative species within the membrane, effectively mitigating radical-induced degradation while maintaining proton conductivity, thereby demonstrating superior chemical durability and long-term fuel cell performance.

Similarly, nanocomposite approaches using functionalized graphene oxide (GO) or other two-dimensional fillers have been shown to improve both chemical and mechanical resilience. Functionalized GO/Nafion composites, for instance, exhibit up to fourfold increases in proton conductivity under low humidity and high temperature, while also reducing gas crossover and enhancing membrane stability [161,162]. The use of 2D poly(triazine imide) (PTI) as a multifunctional additive has also been reported to boost proton conductivity by up to 67 % under low RH and improve long-range connectivity, leading to over 55 % increases in current and power densities in practical PEMFCs, simplified scheme showed in Fig. 8f [155].

Besides, cross-linking strategies further reinforce the membrane structure by creating covalent bonds between polymer chains, which restrict segmental mobility and prevent crack initiation, the primary precursor to pinhole formation. For instance, radiation-induced reversible addition–fragmentation chain transfer (RAFT) polymerization enables the fabrication of well-defined cross-linked PEMs with enhanced structural homogeneity. This nanoscale network uniformity reduces localized stress concentrations during hydration/dehydration cycles, while the covalent cross-links act as barriers against radical-induced chain scission [163]. These improvements stem from the synergistic effect of suppressed mechanical fatigue (via restricted chain slippage) and mitigated chemical attack (via stabilized ionic domains).

These composite and cross-linked membranes demonstrate that rational material design at the nano- and molecular scale can simultaneously address the dual challenges of mechanical fatigue and chemical attack, providing a robust pathway to suppress pinhole formation and extend membrane lifetime.

5.3. Surface modification strategies

5.3.1. Plasma treatment

This method has emerged as a promising technique for surface modification of membranes, offering a solvent-free approach with potential for industrial-scale application and the ability to selectively alter surface properties without impacting the bulk characteristics of the material [156,164–166]. However, its effectiveness remains a subject of debate. According to the study by Barbosa [156], plasma modification can enhance interfacial adhesion due to increased surface roughness and the introduction of oxidative groups. Nevertheless, it may also disrupt the membrane's polymer chain structure, as illustrated in Fig. 8g, where defluorination and the cleavage of sulfonic acid groups were observed, both of which adversely affect ion transport performance. In contrast, a recent study by Heo et al. [164] successfully employed Ar/O_2 plasma treatment to improve membrane performance. Remarkably, after 4800 wet/dry cycles, the plasma-treated membranes retained 94–95 % of their initial performance, whereas untreated samples only maintained 87–89 %, clearly demonstrating enhanced mechanical and chemical durability. The key lies in optimizing the Ar/O_2 plasma dose, which enables effective tailoring of membrane properties, resulting in improved proton conductivity and reduced hydrogen crossover. These findings suggest that plasma treatment demonstrates potential as an effective surface engineering strategy, though further optimization will be essential when applying it to different types of polymer electrolyte membranes.

5.3.2. Chemical grafting

In addition to improving the overall chemical durability, chemical grafting is also considered a promising strategy to mitigate the formation of pinholes. As discussed in the section on chemical degradation, pinholes are known to result from the breakdown of polymer chains caused by free radicals generated during fuel cell operation. Therefore, grafting free radical scavengers onto the polymer backbone not only helps suppress chain-scission reactions, but also contributes to maintaining the structural integrity of the membrane over time. As a result, the membrane is better protected against localized degradation, thereby reducing the likelihood of pinhole initiation and growth.

In the study by Wang et al. [167], organic free radical scavengers such as 2-mercapto-1-methylimidazole (MIm) and 3-mercapto-1,2,4-triazole (MTz) were chemically grafted onto the PAES polymer backbone

to enhance the chemical stability of the membrane. The results showed that PAES-MIm and PAES-MTz membranes retained more than 80 % of their mass after over 500 h of exposure to harsh Fenton conditions, while maintaining good tensile strength, proton conductivity, and fuel cell performance. This demonstrates that chemical grafting of antioxidant groups is an effective approach to enhance the chemical stability and anti-degradation properties of membranes under fuel cell operating conditions.

It is important not to confuse this method with additive blending or doping, although both techniques are aimed at improving membrane properties [167–169]. While chemical grafting involves forming permanent covalent bonds between functional groups and the polymer backbone, additive blending is typically a physical or physicochemical process. As such, grafting tends to offer long-term stability and durability, although it is generally more complex and labor-intensive to implement.

5.4. Simulation- and artificial intelligence (AI)-assisted approaches

Recent advances in simulation and machine learning techniques have opened new opportunities to accelerate research on fuel cell degradation [170–173]. Unlike conventional experimental strategies, which are often time-consuming and resource-intensive, simulation and AI-based approaches can extract degradation patterns, identify hidden correlations among operational parameters, and provide predictive insights that guide targeted experiments [174]. These methods are increasingly regarded as essential tools for prognostics and health management of PEMFCs, complementing empirical studies and enabling more efficient design and optimization of membranes [175].

The works of Zhang et al. have systematically demonstrated how combining mechanistic models with machine learning frameworks can enhance the reliability of PEMFC prognostics [176–179]. Their studies range from the development of replacement models to optimize operating strategies [179], to hybrid frameworks that integrate electrochemical degradation models, filtering algorithms, and advanced neural networks for long-term durability prediction [177], as well as signal-processing-assisted machine learning models for short-term performance forecasting under practical operating conditions [176,178]. Taken together, these efforts illustrate how integrated simulation-AI approaches can capture nonlinear degradation processes, reduce reliance on extensive experimentation, and provide valuable insights into membrane failure analysis.

Although current applications mainly focus on general durability and health management, the same methodology shows great potential for pinhole-related research. Pinhole formation is inherently random, driven by coupled chemical, mechanical, and thermal stressors that act across multiple scales. Traditional post-mortem characterization offers only limited predictive insight. In contrast, simulation–AI frameworks could bridge this gap by linking operational histories, local stress fields, and in-situ diagnostic signals with pinhole initiation and propagation. By combining mechanistic models of membrane degradation with machine learning trained on experimental datasets, it may become possible to identify likely nucleation sites, estimate growth kinetics, and develop proactive strategies to mitigate pinhole formation. Such approaches would also support rational materials design, accelerating the discovery of pinhole-resistant ionomers, nanocomposites, and surface modification strategies.

Overall, simulation- and AI-assisted approaches represent a promising fourth pillar alongside polymer chemistry modifications, composite/nanostructured membranes, and surface engineering. Their integration into pinhole research may not only reduce experimental burdens but also provide predictive power, enabling real-time monitoring and predictive maintenance of PEMFCs. As PEMFCs move toward large-scale commercialization, these digital tools will become increasingly indispensable for ensuring the durability and safety of next-generation membranes.

5.5. Comparative assessment of mitigation strategies

To elucidate the distinctions among the aforementioned mitigation strategies, Table 5 summarizes their respective advantages, limitations, and suitability for practical PEMFC operation. While each approach addresses specific aspects of pinhole suppression, their effectiveness and scalability depend strongly on the balance between chemical durability, mechanical robustness, and manufacturability.

Collectively, these strategies reveal that suppressing pinhole formation in PEMs demands more than isolated material improvements. The convergence of chemical stabilization, mechanical reinforcement, and interfacial optimization has proven essential, yet no single route fully resolves the durability–conductivity trade-off. Continued progress will rely on integrating these complementary approaches under a unified design framework, supported by predictive modeling and in-situ diagnostics to bridge fundamental understanding with practical reliability.

6. Summary and outlook

The long-term PEM durability remains the central challenge to the widespread deployment of PEMFCs, particularly under dynamic, real-world conditions. This review has outlined the interrelated chemical, mechanical, and thermal degradation pathways leading to membrane thinning, loss of conductivity, and ultimately the formation of pinholes—a primary failure mode responsible for performance decline and safety risks in PEMFC systems—have been discussed. Although considerable progress has been made in understanding these failure mechanisms, and in developing mitigation strategies such as radical scavengers, reinforced composites, and surface treatments, most of these approaches target isolated failure modes. However, in fuel cell operation under practical conditions, degradation is rarely driven by a single factor. Localized hotspots, hydration cycling, radical attack, and mechanical fatigue often occur simultaneously and interact in complex, non-linear ways.

Therefore, for future advancements, a more comprehensive and multifunctional membrane design philosophy is needed. This includes the integration of robust polymer backbones, nanostructured reinforcement, adaptive interfacial architectures, and thermal regulation. Emerging concepts like self-healing membranes and responsive polymer systems, which can dynamically recover from damage or reinforce stress-prone areas, represent an exciting shift from passive resistance to active durability. Equally important, simulation- and artificial intelligence-assisted approaches are emerging as a powerful complementary strategy. By integrating multiphysics modeling, data-driven prediction, and machine-learning-based optimization, these tools can quantitatively correlate operational stressors with membrane degradation kinetics, identify early signs of pinhole initiation, and accelerate the discovery of durable ionomers and interfacial architectures. The synergy between experimental diagnostics and digital modeling will be vital for predictive maintenance and for establishing standardized, simulation-guided design protocols.

On the implementation side, most materials developed to date remain at the lab scale. To translate these into viable commercial solutions, researchers must consider scalability, compatibility with industrial fabrication methods, and long-term performance under standardized testing protocols. It is particularly important to ensure that reported durability improvements are not condition-specific, and that the results are reproducible across different testing setups. In this regard, closer collaboration between academia and industry will be essential, not only to validate high-performing materials but also to bridge the gap between innovation and manufacturability.

In conclusion, addressing pinhole formation in PEMs requires more than solving an isolated degradation problem, it requires efforts ranging from molecular modification to a system-level approach, one that anticipates interaction between multiple stressors, balances competing

Table 5
Comparative assessment of strategies for mitigating pinhole formation and propagation in PEMs.

Strategy	Key Mechanism	Advantages	Limitations	Ref.
Polymer chemistry modification	Structural optimization and dynamic chain repair	Excellent proton conductivity and oxidation resistance; long-term chemical stability	Complex synthesis routes; limited recovery after repeated damage	[150–152]
Composite/nanostructured membranes	Inorganic reinforcement and interfacial bonding	Enhanced mechanical strength; reduced gas crossover; adaptable formulations	Potential filler aggregation; reduced flexibility	[32, 160–162]
Surface modification (plasma, chemical grafting)	Surface chemistry tailoring and radical scavenging	Simple processing; scalable; effective in reducing surface defects	Risk of over-oxidation or chain scission; limited penetration depth	[164,167]
Simulation- and AI-assisted design	Predictive modeling and degradation mapping	Non-destructive; accelerates optimization; enables predictive maintenance	Requires extensive datasets; limited by model generalizability	[176–179]

design trade-offs, and align scientific exploration with practical operational constraints. Looking ahead, the next generation of fuel cell systems will depend on membranes that combine durability, functional versatility, and the capacity to adapt to internal stress and damage over time.

CRediT authorship contribution statement

Cam-Tu Hoang-Ngoc: Writing – original draft, Formal analysis, Conceptualization. **Sang Moon Kim:** Writing – review & editing, Supervision, Project administration, Conceptualization.

Declaration of competing interest

The authors declare that they have no known competing financial interests or personal relationships that could have appeared to influence the work reported in this paper.

Acknowledgements

This work was supported by the National Research Foundation (NRF) of Korea (RS-2025-02482982 and RS-2023-00277319).

Data availability

No data was used for the research described in the article.

References

[1] Intergovernmental Panel on Climate Change, I, Climate change 2023, sixth assessment report (AR6). https://www.ipcc.ch/assessment-report/ar6/, 2023. (Accessed 13 August 2025).
[2] I.E. Agency, World energy outlook 2024. https://www.iea.org/reports/world-energy-outlook-2024, 2024. (Accessed 13 August 2025).
[3] U.S. D.o. Energy, Hydrogen and fuel cell technologies office: multi-year program plan, May 2024, https://www.energy.gov/sites/default/files/2024-05/hfto-mypp-fuel-cell-technologies.pdf, 2024. (Accessed 13 August 2025).
[4] U.S. D.o. Energy, Hydrogen and fuel cell technologies office multi-year program plan: systems development and integration. https://www.energy.gov/sites/default/files/2024-05/hfto-mypp-systems-development-integration.pdf, 2024. (Accessed 13 August 2025).
[5] X. Fu, J. Wang, F. Peng, Y. Wang, S. Hu, R. Zhang, Q. Liu, Int. J. Hydrogen Energy 48 (42) (2023) 16072–16082, https://doi.org/10.1016/j.ijhydene.2023.01.087.
[6] G. Shen, J. Liu, H.B. Wu, P. Xu, F. Liu, C. Tongsh, K. Jiao, J. Li, M. Liu, M. Cai, Nat. Commun. 11 (1) (2020) 1191, https://doi.org/10.1038/s41467-020-14822-y.
[7] C. Kim, Y. Na, Renew. Energy 241 (2025) 122315, https://doi.org/10.1016/j.renene.2024.122315.
[8] M.J. Parnian, S. Rowshanzamir, A.K. Prasad, S.G. Advani, J. Membr. Sci. 556 (2018) 12–22, https://doi.org/10.1016/j.memsci.2018.03.083.
[9] W. Zeng, B. Guan, Z. Zhuang, J. Chen, L. Zhu, Z. Ma, X. Hu, C. Zhu, S. Zhao, K. Shu, et al., Int. J. Hydrogen Energy 102 (2025) 222–246, https://doi.org/10.1016/j.ijhydene.2024.12.513.
[10] M.P. Rodgers, L.J. Bonville, H.R. Kunz, D.K. Slattery, J.M. Fenton, Chem. Rev. 112 (11) (2012) 6075–6103, https://doi.org/10.1021/cr200424d.
[11] M. Raja Pugalenthi, K. Punyawudho, M. Anbu Arasi, A.A. Shah, M. Ramesh Prabhu, M. Kouthaman, K. Velsankar, R. Gayathri, Mater. Lett. 339 (2023) 134117, https://doi.org/10.1016/j.matlet.2023.134117.
[12] S. Wen, C. Gong, W.-C. Tsen, Y.-C. Shu, F.-C. Tsai, Int. J. Hydrogen Energy 34 (21) (2009) 8982–8991, https://doi.org/10.1016/j.ijhydene.2009.08.074.
[13] T.K. Maiti, J. Singh, J. Majhi, A. Ahuja, S. Maiti, P. Dixit, S. Bhushan, A. Bandyopadhyay, S. Chattopadhyay, Polymer 255 (2022) 125151, https://doi.org/10.1016/j.polymer.2022.125151.
[14] R.E. Rosli, A.B. Sulong, W.R.W. Daud, M.A. Zulkifley, T. Husaini, M.I. Rosli, E. H. Majlan, M.A. Haque, Int. J. Hydrogen Energy 42 (14) (2017) 9293–9314, https://doi.org/10.1016/j.ijhydene.2016.06.211.
[15] U.S. D.o. Energy, DOE Technical Targets for Fuel Cell Systems and Stacks for Transportation Applications, U.S. Department of Energy, Office of Energy Efficiency & Renewable Energy, 2022. https://www.energy.gov/eere/fuelcells/doe-technical-targets-fuel-cell-systems-and-stacks-transportation-applications, 2025-07-23.
[16] P. Pei, Y. Meng, D. Chen, P. Ren, M. Wang, X. Wang, Energy 265 (2023) 126341, https://doi.org/10.1016/j.energy.2022.126341.
[17] X. Zhao, Y. Zhou, L. Wang, B. Pan, R. Wang, L. Wang, Int. J. Hydrogen Energy 48 (57) (2023) 21864–21885, https://doi.org/10.1016/j.ijhydene.2023.03.033.
[18] S.T. Putnam, J. Rodríguez-López, Chem. Sci. 15 (26) (2024) 10036–10045, https://doi.org/10.1039/D4SC01553C.
[19] X. Qi, X. Gao, H. Zhang, Y. Qiu, R. Zhang, P.-C. Sui, Int. J. Hydrogen Energy 95 (2024) 1011–1021, https://doi.org/10.1016/j.ijhydene.2024.11.222.
[20] L. Marcelli, D. Chamoret, X. François, Y. Meyer, D. Candusso, Int. J. Hydrogen Energy 136 (2025) 1086–1111, https://doi.org/10.1016/j.ijhydene.2025.03.004.
[21] R. Shimizu, J. Tsuji, N. Sato, J. Takano, S. Itami, M. Kusakabe, K. Miyatake, A. Iiyama, M. Uchida, J. Power Sources 367 (2017) 63–71, https://doi.org/10.1016/j.jpowsour.2017.09.025.
[22] C.S. Gittleman, F.D. Coms, Y.-H. Lai, Membrane durability: physical and chemical degradation, in: Polymer Electrolyte Fuel Cell Degradation, vol. 15, Elsevier Science, Burlington, 2011.
[23] F. Ding, T. Zou, T. Wei, L. Chen, X. Qin, Z. Shao, J. Yang, Appl. Energy 342 (2023) 121136, https://doi.org/10.1016/j.apenergy.2023.121136.
[24] B.T. Huang, Y. Chatillon, C. Bonnet, F. Lapicque, S. Leclerc, M. Hinaje, S. Raël, Int. J. Hydrogen Energy 38 (1) (2013) 543–550, https://doi.org/10.1016/j.ijhydene.2012.09.058.
[25] V. Stanic, M. Hoberecht, ECS proceedings volumes 2004, 1, 391, https://doi.org/10.1149/200421.0391PV, 2004.
[26] M. Bodner, C. Hochenauer, V. Hacker, J. Power Sources 295 (2015) 336–348, https://doi.org/10.1016/j.jpowsour.2015.07.021.
[27] S. Kreitmeier, M. Michiardi, A. Wokaun, F.N. Büchi, Electrochim. Acta 80 (2012) 240–247, https://doi.org/10.1016/j.electacta.2012.07.013.
[28] S. Kreitmeier, P. Lerch, A. Wokaun, F.N. Büchi, J. Electrochem. Soc. 160 (4) (2013), https://doi.org/10.1149/1.023306jes. F456.
[29] Energy, U. S. D. o., Fuel Cell Technical Team Roadmap (2017). November 2017, https://www.energy.gov/sites/prod/files/2017/11/f46/FCTT_Roadmap_Nov_2017.pdf. (Accessed 30 September 2025).
[30] A.M. Niroumand, H. Homayouni, G. Goransson, M. Olfert, M. Eikerling, J. Power Sources 448 (2020) 227359, https://doi.org/10.1016/j.jpowsour.2019.227359.
[31] X. Yu, S. Bai, Q. Li, Z. Zhao, Q. Sun, S. Cao, H. Cui, M. Liu, Q. Xu, C.-C. Hou, Energy 7 (1) (2025) 100142, https://doi.org/10.1016/j.enchem.2024.100142.
[32] B. Liu, Y. Duan, Y. Pang, Q. Li, C. Zhao, Chem. Eng. J. 477 (2023) 146955, https://doi.org/10.1016/j.cej.2023.146955.
[33] O.A. Obewhere, K. Acurio-Cerda, S. Sutradhar, M. Dike, R. Keloth, S.K. Dishari, Chem. Commun. 60 (90) (2024) 13114–13142, https://doi.org/10.1039/D4CC03221G.
[34] M. Arun, S. Giddey, P. Joseph, D.S. Dhawale, J. Mater. Chem. A 13 (16) (2025) 11236–11263, https://doi.org/10.1039/D4TA08823A.
[35] S.A. Grigoriev, K.A. Dzhus, D.G. Bessarabov, P. Millet, Int. J. Hydrogen Energy 39 (35) (2014) 20440–20446, https://doi.org/10.1016/j.ijhydene.2014.05.043.
[36] L. Placca, R. Kouta, Int. J. Hydrogen Energy 36 (19) (2011) 12393–12405, https://doi.org/10.1016/j.ijhydene.2011.06.093.
[37] E. Wallnöfer-Ogris, F. Poimer, R. Köll, M.-G. Macherhammer, A. Trattner, Int. J. Hydrogen Energy 50 (2024) 1159–1182, https://doi.org/10.1016/j.ijhydene.2023.06.215.
[38] Y.-H. Lai, G.W. Fly, J. Power Sources 274 (2015) 1162–1172, https://doi.org/10.1016/j.jpowsour.2014.10.116.
[39] E. Wallnöfer-Ogris, I. Grimmer, M. Ranz, M. Höglinger, S. Kartusch, J. Rauh, M.-G. Macherhammer, B. Grabner, A. Trattner, Int. J. Hydrogen Energy 65 (2024) 381–397, https://doi.org/10.1016/j.ijhydene.2024.04.017.
[40] S. Kundu, M.W. Fowler, L.C. Simon, S. Grot, J. Power Sources 157 (2) (2006) 650–656, https://doi.org/10.1016/j.jpowsour.2005.12.027.
[41] T. Uchiyama, H. Kumei, T. Yoshida, K. Ishihara, J. Power Sources 272 (2014) 522–530, https://doi.org/10.1016/j.jpowsour.2014.08.103.

[42] D.H. Ye, Z.G. Zhan, Y.J. Lee, Z.K. Tu, Y. Zhang, M. Pan, Fuel Cells 13 (6) (2013) 1205–1212, https://doi.org/10.1002/fuce.201300073.
[43] R. Gadhewal, V. Vinod Ananthula, V. Suresh Patnaikuni, Mater. Today Proc. 72 (2023) 410–416, https://doi.org/10.1016/j.matpr.2022.08.190.
[44] Y. Xing, H. Li, G. Avgouropoulos, Materials 14 (10) (2021) 2591, https://doi.org/10.3390/ma14102591.
[45] G. De Moor, C. Bas, N. Charvin, E. Moukheiber, F. Niepceron, N. Breilly, J. André, E. Rossinot, E. Claude, N.D. Albérola, et al., Fuel Cells 12 (3) (2012) 356–364, https://doi.org/10.1002/fuce.201100161.
[46] Q. Wang, B. Li, D. Yang, H. Dai, J.P. Zheng, P. Ming, C. Zhang, J. Power Sources 492 (2021) 229613, https://doi.org/10.1016/j.jpowsour.2021.229613.
[47] S. Yuan, C. Zhao, X. Cai, L. An, S. Shen, X. Yan, J. Zhang, Prog. Energy Combust. Sci. 96 (2023) 101075, https://doi.org/10.1016/j.pecs.2023.101075.
[48] V. Patil, P.V. Reshmi, S. Prajna, Yashaswini Yashaswi, D. Haleshappa, A. Jayarama, R. Pinto, Mater. Today Proc. (2023), https://doi.org/10.1016/j.matpr.2023.03.603.
[49] C. Chen, T.F. Fuller, Polym. Degrad. Stabil. 94 (9) (2009) 1436–1447, https://doi.org/10.1016/j.polymdegradstab.2009.05.016.
[50] A.A. Shah, T.R. Ralph, F.C. Walsh, J. Electrochem. Soc. 156 (4) (2009), https://doi.org/10.1149/1.3077573. B465.
[51] S. Lee, J. Nam, J. Ahn, S. Yoon, S.C. Jeong, H. Ju, C.H. Lee, Int. J. Hydrogen Energy 96 (2024) 333–342, https://doi.org/10.1016/j.ijhydene.2024.11.319.
[52] D.E. Curtin, R.D. Lousenberg, T.J. Henry, P.C. Tangeman, M.E. Tisack, J. Power Sources 131 (1) (2004) 41–48, https://doi.org/10.1016/j.jpowsour.2004.01.023.
[53] A. Collier, H. Wang, X. Zi Yuan, J. Zhang, D.P. Wilkinson, Int. J. Hydrogen Energy 31 (13) (2006) 1838–1854, https://doi.org/10.1016/j.ijhydene.2006.05.006.
[54] T. Sharma, U. Adhikari, A. Nandimath, J. Pandey, Mater. Today Sustain. 30 (2025) 101103, https://doi.org/10.1016/j.mtsust.2025.101103.
[55] V.O. Mittal, H.R. Kunz, J.M. Fenton, Electrochem. Solid State Lett. 9 (6) (2006), https://doi.org/10.1149/1.2192696. A299.
[56] P. Ren, P. Pei, Y. Li, Z. Wu, D. Chen, S. Huang, Prog. Energy Combust. Sci. 80 (2020) 100859, https://doi.org/10.1016/j.pecs.2020.100859.
[57] K. Hongsirikarn, X. Mo, J.G. Goodwin, S. Creager, J. Power Sources 196 (6) (2011) 3060–3072, https://doi.org/10.1016/j.jpowsour.2010.11.133.
[58] H. Zhang, S. Wu, X. Huang, L. Li, Q. Liao, Z. Wei, Chem. Eng. J. 428 (2022) 131534, https://doi.org/10.1016/j.cej.2021.131534.
[59] C. Chen, T.F. Fuller, Electrochim. Acta 54 (16) (2009) 3984–3995, https://doi.org/10.1016/j.electacta.2009.02.021.
[60] N. Ohguri, A.Y. Nosaka, Y. Nosaka, J. Power Sources 195 (15) (2010) 4647–4652, https://doi.org/10.1016/j.jpowsour.2010.02.010.
[61] R. Maurya, P. Morgen, R. Sharma, S.M. Andersen, J. Power Sources 631 (2025) 236243, https://doi.org/10.1016/j.jpowsour.2025.236243.
[62] E. Colombo, A. Grimaldi, A. Baricci, M. Pak, Y. Morimoto, I.V. Zenyuk, A. Casalegno, J. Power Sources 629 (2025) 235962, https://doi.org/10.1016/j.jpowsour.2024.235962.
[63] K. Xu, G. Liu, X. Xu, Z. Wang, G. Liu, F. Liu, Y. Zhang, Y. Zhou, Y. Zou, S. Pei, J. Membr. Sci. 699 (2024) 122641, https://doi.org/10.1016/j.memsci.2024.122641.
[64] X. Shen, X. Liang, Y. Xu, W. Yu, Q. Li, X. Ge, L. Wu, T. Xu, J. Membr. Sci. 675 (2023) 121556, https://doi.org/10.1016/j.memsci.2023.121556.
[65] R. Lv, S. Jin, L. Li, Q. Wang, L. Wang, J. Wang, J. Yang, J. Membr. Sci. 701 (2024) 122703, https://doi.org/10.1016/j.memsci.2024.122703.
[66] Y. Zhao, B. Lv, W. Song, J. Hao, J. Zhang, Z. Shao, J. Membr. Sci. 674 (2023) 121531, https://doi.org/10.1016/j.memsci.2023.121531.
[67] S. Yang, Y. Zeng, C. Xiao, M. Yang, H. Chen, Q. Liu, W. Huang, Y. Gong, S. Peng, J. Membr. Sci. 722 (2025) 123867, https://doi.org/10.1016/j.memsci.2025.123867.
[68] H.S. Thiam, W.R.W. Daud, S.K. Kamarudin, A.B. Mohammad, A.A.H. Kadhum, K. S. Loh, E.H. Majlan, Int. J. Hydrogen Energy 36 (4) (2011) 3187–3205, https://doi.org/10.1016/j.ijhydene.2010.11.062.
[69] A. Kusoglu, A.Z. Weber, Chem. Rev. 117 (3) (2017) 987–1104, https://doi.org/10.1021/acs.chemrev.6b00159.
[70] K.D. Kreuer, J. Membr. Sci. 185 (1) (2001) 29–39, https://doi.org/10.1016/S0376-7388(00)00632-3.
[71] G. Xu, A. Ke, F. Ji, Y. Liu, Z. Zhao, R. Lv, B. Huang, J. Li, C. Deng, Y. Sun, et al., Fuel 361 (2024) 130706, https://doi.org/10.1016/j.fuel.2023.130706.
[72] M.R. Asghar, W. Zhang, H. Su, J. Zhang, B. Rhimi, H. Liu, L. Xing, X. Yan, Q. Xu, J. Power Sources 622 (2024) 235353, https://doi.org/10.1016/j.jpowsour.2024.235353.
[73] A. Kato, S. Yamaguchi, W. Yoshimune, K. Isegawa, M. Maeda, D. Hayashi, T. Suzuki, S. Kato, Electrochem. Commun. 165 (2024) 107772, https://doi.org/10.1016/j.elecom.2024.107772.
[74] M. Bogar, Y. Yakovlev, S. Pollastri, R. Biagi, H. Amenitsch, R. Taccani, I. Matolínová, J. Power Sources 615 (2024) 235070, https://doi.org/10.1016/j.jpowsour.2024.235070.
[75] Y. Wu, L. Xu, S. Zhou, J. Yang, W. Kockelmann, Y. Han, Q. Li, W. Chen, M. O. Coppens, P.R. Shearing, et al., Appl. Energy 364 (2024) 123204, https://doi.org/10.1016/j.apenergy.2024.123204.
[76] Y. Yang, J. Feijóo, V. Briega-Martos, Q. Li, M. Krumov, S. Merkens, G. De Salvo, A. Chuvilin, J. Jin, H. Huang, et al., Curr. Opin. Electrochem. 42 (2023) 101403, https://doi.org/10.1016/j.coelec.2023.101403.
[77] M. Bogar, Y. Yakovlev, J. Nováková, A.M. Darabut, M. Kriechbaum, H. Amenitsch, R. Taccani, I. Matolínová, Int. J. Hydrogen Energy 58 (2024) 1673–1681, https://doi.org/10.1016/j.ijhydene.2024.01.261.
[78] M. Haslinger, T. Lauer, J. Power Sources 606 (2024) 234523, https://doi.org/10.1016/j.jpowsour.2024.234523.
[79] D. Madhav, J. Wang, R. Keloth, J. Mus, F. Buysschaert, V. Vandeginste, Energies 17 (2024) 5, https://doi.org/10.3390/en17050998.
[80] S. Shi, X. Sun, Q. Lin, J. Chen, Y. Fu, X. Hong, C. Li, X. Guo, G. Chen, X. Chen, Int. J. Hydrogen Energy 45 (51) (2020) 27653–27664, https://doi.org/10.1016/j.ijhydene.2020.07.113.
[81] Y.-H. Lai, C.K. Mittelsteadt, C.S. Gittleman, D.A. Dillard, Viscoelastic stress model and mechanical characterization of perfluorosulfonic acid (PFSA) polymer electrolyte membranes, in: 3rd International Conference on Fuel Cell Science, Engineering and Technology, 37645, 2005, pp. 161–167, https://doi.org/10.1115/FUELCELL2005-74120. Ypsilanti, Michigan, USA, 2005.
[82] D. Ramani, Y. Singh, R.T. White, M. Wegener, F.P. Orfino, M. Dutta, E. Kjeang, Int. J. Hydrogen Energy 45 (16) (2020) 10089–10103, https://doi.org/10.1016/j.ijhydene.2020.02.013.
[83] S. Shi, J. Li, H. Li, Y. Yao, H. Dai, Y. Fu, Q. Lin, X. Chen, Int. J. Fatig. 154 (2022) 106554, https://doi.org/10.1016/j.ijfatigue.2021.106554.
[84] Q. Yan, H. Toghiani, Y.-W. Lee, K. Liang, H. Causey, J. Power Sources 160 (2) (2006) 1242–1250, https://doi.org/10.1016/j.jpowsour.2006.02.075.
[85] D. Liu, S. Case, J. Power Sources 162 (1) (2006) 521–531, https://doi.org/10.1016/j.jpowsour.2006.07.007.
[86] M. Jouin, R. Gouriveau, D. Hissel, M.-C. Péra, N. Zerhouni, Reliab. Eng. Syst. Saf. 148 (2016) 78–95, https://doi.org/10.1016/j.ress.2015.12.003.
[87] D. Qiu, L. Peng, P. Liang, P. Yi, X. Lai, Energy 165 (2018) 210–222, https://doi.org/10.1016/j.energy.2018.09.136.
[88] P.C. Okonkwo, I. Ben Belgacem, W. Emori, P.C. Uzoma, Int. J. Hydrogen Energy 46 (55) (2021) 27956–27973, https://doi.org/10.1016/j.ijhydene.2021.06.032.
[89] Q. Duan, H. Wang, J. Benziger, J. Membr. Sci. 392–393 (2012) 88–94, https://doi.org/10.1016/j.memsci.2011.12.004.
[90] S. Hommura, K. Kawahara, T. Shimohira, Y. Teraoka, J. Electrochem. Soc. 155 (2007), https://doi.org/10.1149/1.2800171, 1, A29.
[91] B. Wu, M. Zhao, W. Shi, W. Liu, J. Liu, D. Xing, Y. Yao, Z. Hou, P. Ming, J. Gu, et al., Int. J. Hydrogen Energy 39 (26) (2014) 14381–14390, https://doi.org/10.1016/j.ijhydene.2014.02.142.
[92] L. Ghassemzadeh, K.D. Kreuer, J. Maier, K. Müller, J. Power Sources 196 (5) (2011) 2490–2497, https://doi.org/10.1016/j.jpowsour.2010.11.053.
[93] M. Danilczuk, S. Schlick, F.D. Coms, Degradation mechanism of perfluorinated membranes, in: S. Schlick (Ed.), The Chemistry of Membranes Used in Fuel Cells: Degradation and Stabilization, Wiley Online Library, 2018, pp. 19–53.
[94] M. Maier, D. Abbas, J. Mitrovic, A. Marth, S. Thiele, T. Böhm, ACS Appl. Energy Mater. 7 (22) (2024) 10637–10649, https://doi.org/10.1021/acsaem.4c02241.
[95] J.H. Lim, J. Hou, C.H. Lee, Polymers 13 (23) (2021) 4177, https://doi.org/10.3390/polym13234177.
[96] L. Ghassemzadeh, K.-D. Kreuer, J. Maier, K. Muller, J. Phys. Chem. C 114 (34) (2010) 14635–14645, https://doi.org/10.1021/jp102533v.
[97] Y. Li, D.A. Dillard, S.W. Case, M.W. Ellis, Y.-H. Lai, C.S. Gittleman, D.P. Miller, J. Power Sources 194 (2) (2009) 873–879, https://doi.org/10.1016/j.jpowsour.2009.06.083.
[98] P.M. Ngo, T. Karimata, T. Saitou, K. Ito, J. Power Sources 556 (2023) 232446, https://doi.org/10.1016/j.jpowsour.2022.232446.
[99] W. Ming, P. Sun, Z. Zhang, W. Qiu, J. Du, X. Li, Y. Zhang, G. Zhang, K. Liu, Y. Wang, et al., Int. J. Hydrogen Energy 48 (13) (2023) 5197–5228, https://doi.org/10.1016/j.ijhydene.2022.10.261.
[100] E.J.F. Dickinson, G. Smith, Membranes 10 (11) (2020) 310, https://doi.org/10.3390/membranes10110310.
[101] D. Qiu, L. Peng, X. Lai, M. Ni, W. Lehnert, Renew. Sustain. Energy Rev. 113 (2019) 109289, https://doi.org/10.1016/j.rser.2019.109289.
[102] Y. Singh, F.P. Orfino, M. Dutta, E. Kjeang, J. Power Sources 345 (2017) 1–11, https://doi.org/10.1016/j.jpowsour.2017.01.129.
[103] F. Peng, J. Zou, J. Chen, M. Wang, M. Wu, J. Power Sources 645 (2025) 237219, https://doi.org/10.1016/j.jpowsour.2025.237219.
[104] V.O. Mittal, H.R. Kunz, J.M. Fenton, J. Electrochem. Soc. 154 (2007), https://doi.org/10.1149/1.2734869, 7, B652.
[105] T. Schuler, T.J. Schmidt, F.N. Büchi, J. Electrochem. Soc. 166 (10) (2019) F555–F565, https://doi.org/10.1149/2.1241908jes.
[106] H.-Y. Jung, J.W. Kim, Int. J. Hydrogen Energy 37 (17) (2012) 12580–12585, https://doi.org/10.1016/j.ijhydene.2012.05.121.
[107] X. Huang, J. Yan, M. Zhang, Y. Wang, Y. Chen, X. Fu, R. Wei, X.-l. Zheng, Z. Liu, X. Zhang, et al., Cell 175 (1) (2018) 186–199.e119, https://doi.org/10.1016/j.cell.2018.08.058.
[108] R. Borup, J. Meyers, B. Pivovar, Y.S. Kim, R. Mukundan, N. Garland, D. Myers, M. Wilson, F. Garzon, D. Wood, et al., Chem. Rev. 107 (10) (2007) 3904–3951, https://doi.org/10.1021/cr050182l.
[109] Y. Yu, Q. Yu, R. Luo, S. Chen, J. Yang, F. Yan, Int. J. Hydrogen Energy 71 (2024) 1090–1103, https://doi.org/10.1016/j.ijhydene.2024.05.338.
[110] X. Zhang, H. Liao, L. Huang, R. Huang, L. Lin, Y. Jiang, W. Liu, Renew. Energy 241 (2025) 122314, https://doi.org/10.1016/j.renene.2024.122314.
[111] P. Schneider, A.-C. Scherzer, L. Ney, H.-K. Kwon, B.D. Storey, D. Gerteisen, N. Zamel, Sci. Data 11 (1) (2024) 828, https://doi.org/10.1038/s41597-024-03662-w.
[112] C. Liu, J. Wrubel, E. Padgett, G. Bender, J. Power Sources 581 (2023) 233507, https://doi.org/10.1016/j.jpowsour.2023.233507.
[113] J. Hong, J. Yang, Z. Weng, F. Ma, F. Liang, C. Zhang, J. Power Sources 617 (2024) 235118, https://doi.org/10.1016/j.jpowsour.2024.235118.
[114] A.K. Taylor, C. Smith, K.C. Neyerlin, J. Power Sources 571 (2023) 232971, https://doi.org/10.1016/j.jpowsour.2023.232971.
[115] R. Mohsen, T. Olewski, A. Badreldin, A. Abdel-Wahab, L. Véchot, Renew. Sustain. Energy Rev. 211 (2025) 115225, https://doi.org/10.1016/j.rser.2024.115225.

[116] M. Chandesris, R. Vincent, L. Guetaz, J.S. Roch, D. Thoby, M. Quinaud, Int. J. Hydrogen Energy 42 (12) (2017) 8139–8149, https://doi.org/10.1016/j.ijhydene.2017.02.116.
[117] G. De Moor, C. Bas, N. Charvin, E. Moukheiber, F. Niepceron, N. Breilly, J. André, E. Rossinot, E. Claude, N.D. Albérola, Fuel Cells 12 (3) (2012) 356–364, https://doi.org/10.1002/fuce.201100161.
[118] A. Phillips, M. Ulsh, K.C. Neyerlin, J. Porter, G. Bender, Int. J. Hydrogen Energy 43 (12) (2018) 6390–6399, https://doi.org/10.1016/j.ijhydene.2018.02.050.
[119] P.K. Das, A.Z. Weber, G. Bender, A. Manak, D. Bittinat, A.M. Herring, M. Ulsh, J. Power Sources 261 (2014) 401–411, https://doi.org/10.1016/j.jpowsour.2013.11.124.
[120] M. Ulsh, A. DeBari, J.M. Berliner, I.V. Zenyuk, P. Rupnowski, L. Matvichuk, A. Z. Weber, G. Bender, Int. J. Hydrogen Energy 44 (16) (2019) 8533–8547, https://doi.org/10.1016/j.ijhydene.2018.12.181.
[121] M. Kim, G. Zhang, S. Jang, S. Lee, Z. Suo, S.M. Kim, Adv. Mater. 36 (14) (2024) 2308288, https://doi.org/10.1002/adma.202308288.
[122] S.R. Choi, D.Y. Kim, W.Y. An, S. Choi, K. Park, S.-D. Yim, J.-Y. Park, Mater. Sci. Energy Technol. 5 (2022) 66–73, https://doi.org/10.1016/j.mset.2021.12.001.
[123] S. Kreitmeier, G.A. Schuler, A. Wokaun, F.N. Büchi, J. Power Sources 212 (2012) 139–147, https://doi.org/10.1016/j.jpowsour.2012.03.071.
[124] H. Tao, K. Yang, B. Wang, B. Hou, K. Wu, Z. Qin, B. Luo, J. Kang, Q. Du, K. Jiao, Int. J. Heat Mass Tran. 234 (2024) 126060, https://doi.org/10.1016/j.ijheatmasstransfer.2024.126060.
[125] M. Inaba, T. Kinumoto, M. Kiriake, R. Umebayashi, A. Tasaka, Z. Ogumi, Electrochim. Acta 51 (26) (2006) 5746–5753, https://doi.org/10.1016/j.electacta.2006.03.008.
[126] H. Zhang, J. Li, H. Tang, Y. Lin, M. Pan, Int. J. Hydrogen Energy 39 (28) (2014) 15989–15995, https://doi.org/10.1016/j.ijhydene.2014.01.076.
[127] J. Wu, X.Z. Yuan, H. Wang, M. Blanco, J.J. Martin, J. Zhang, Int. J. Hydrogen Energy 33 (6) (2008) 1735–1746, https://doi.org/10.1016/j.ijhydene.2008.01.013.
[128] P. Pei, Z. Wu, Y. Li, X. Jia, D. Chen, S. Huang, Appl. Energy 215 (2018) 338–347, https://doi.org/10.1016/j.apenergy.2018.02.002.
[129] H. Gunji, M. Eguchi, F. Sekine, Y. Tsutsumi, Int. J. Hydrogen Energy 42 (1) (2017) 562–574, https://doi.org/10.1016/j.ijhydene.2016.11.038.
[130] S.A. Vilekar, R. Datta, J. Power Sources 195 (8) (2010) 2241–2247, https://doi.org/10.1016/j.jpowsour.2009.10.023.
[131] Q. Tang, B. Li, D. Yang, P. Ming, C. Zhang, Y. Wang, Int. J. Hydrogen Energy 46 (42) (2021) 22040–22061, https://doi.org/10.1016/j.ijhydene.2021.04.050.
[132] C. Ji, H. Niu, S. Wang, C. Liang, X. Li, J. Yang, Int. J. Energy Res. 43 (7) (2019) 2881–2896, https://doi.org/10.1002/er.4430.
[133] S. Zhang, X.-Z. Yuan, R. Hiesgen, K.A. Friedrich, H. Wang, M. Schulze, A. Haug, H. Li, J. Power Sources 205 (2012) 290–300, https://doi.org/10.1016/j.jpowsour.2012.01.031.
[134] R. O'hayre, S.-W. Cha, W. Colella, F.B. Prinz, Fuel Cell Fundamentals, John Wiley & Sons, 2016.
[135] K.R. Cooper, Experimental Methods and Data Analyses for Polymer Electrolyte Fuel Cells, Scribner Associates, 2005.
[136] G. De Moor, C. Bas, N. Charvin, J. Dillet, G. Maranzana, O. Lottin, N. Caqué, E. Rossinot, L. Flandin, Int. J. Hydrogen Energy 41 (1) (2016) 483–496, https://doi.org/10.1016/j.ijhydene.2015.10.066.
[137] S. Asghari, B. Fouladi, N. Masaeli, B.F. Imani, Int. J. Hydrogen Energy 39 (27) (2014) 14980–14992, https://doi.org/10.1016/j.ijhydene.2014.07.044.
[138] X.-Z. Yuan, S. Zhang, S. Ban, C. Huang, H. Wang, V. Singara, M. Fowler, M. Schulze, A. Haug, K. Andreas Friedrich, et al., J. Power Sources 205 (2012) 324–334, https://doi.org/10.1016/j.jpowsour.2012.01.074.
[139] M. Obermaier, K. Jozwiak, M. Rauber, A. Bauer, C. Scheu, J. Power Sources 488 (2021) 229405, https://doi.org/10.1016/j.jpowsour.2020.229405.
[140] Q. Meyer, Y. Zeng, C. Zhao, J. Power Sources 437 (2019) 226922, https://doi.org/10.1016/j.jpowsour.2019.226922.
[141] J. Zuo, N.Y. Steiner, Z. Li, D. Hissel, Appl. Energy 378 (2025) 124762, https://doi.org/10.1016/j.apenergy.2024.124762.
[142] M.V. Paredes, A.G. Manjón, B. Hill, T. Schwarz, N.A. Rivas, T. Jurzinsky, K. Hengge, F. Mack, C. Scheu, Nanoscale 14 (32) (2022) 11543–11551, https://doi.org/10.1039/D2NR02892A.
[143] L. Birkner, M. Foreta, A. Rinaldi, A. Orekhov, M.-G. Willinger, M. Eichelbaum, Sci. Rep. 14 (1) (2024) 3999, https://doi.org/10.1038/s41598-024-54258-8.
[144] G. Bender, W. Felt, M. Ulsh, J. Power Sources 253 (2014) 224–229, https://doi.org/10.1016/j.jpowsour.2013.12.045.
[145] M. Wang, S. Medina, J. Ochoa-Lozano, S. Mauger, S. Pylypenko, M. Ulsh, G. Bender, Int. J. Hydrogen Energy 46 (27) (2021) 14699–14712, https://doi.org/10.1016/j.ijhydene.2021.01.186.
[146] W. Lü, Z. Liu, C. Wang, Z. Mao, M. Zhang, Int. J. Energy Res. 35 (1) (2011) 24–30, https://doi.org/10.1002/er.1728.
[147] H. Lee, T. Kim, W. Sim, S. Kim, B. Ahn, T. Lim, K. Park, Kor. J. Chem. Eng. 28 (2) (2011) 487–491, https://doi.org/10.1007/s11814-010-0381-6.
[148] P. Jiang, F. Wu, W. Yu, Z. Huang, X. Huang, Z. Zhan, S. Li, M. Pan, Chem. Eng. J. 518 (2025) 164666, https://doi.org/10.1016/j.cej.2025.164666.
[149] S. Hegde, R. Wörner, B. Shabani, Int. J. Hydrogen Energy 118 (2025) 268–299, https://doi.org/10.1016/j.ijhydene.2025.02.402.
[150] D. Cha, S.W. Jeon, W. Yang, D. Kim, Y. Kim, Energy 150 (2018) 320–328, https://doi.org/10.1016/j.energy.2018.02.133.
[151] A. Stassi, I. Gatto, E. Passalacqua, V. Antonucci, A.S. Arico, L. Merlo, C. Oldani, E. Pagano, J. Power Sources 196 (21) (2011) 8925–8930, https://doi.org/10.1016/j.jpowsour.2010.12.084.
[152] S. Wang, M.W. Urban, Nat. Rev. Mater. 5 (8) (2020) 562–583, https://doi.org/10.1038/s41578-020-0202-4.
[153] F. Li, H. Xia, J. Appl. Polym. Sci. 135 (13) (2018) 46050, https://doi.org/10.1002/app.46050.
[154] W.W. Ng, H.S. Thiam, Y.L. Pang, Y.S. Lim, J. Wong, L.H. Saw, J. Environ. Chem. Eng. 11 (6) (2023) 111151, https://doi.org/10.1016/j.jece.2023.111151.
[155] K. Smith, F. Foglia, A.J. Clancy, D.J.L. Brett, T.S. Miller, Adv. Funct. Mater. 33 (2023) 42–2304061, https://doi.org/10.1002/adfm.202304061.
[156] R. Barbosa, R. Gonçalves, G.E.O. Blanco, M.C. Saccardo, R.S. Paiva, V. R. Mastelaro, S.A. Cruz, C.H. Scuracchio, J. Power Sources 610 (2024) 234741, https://doi.org/10.1016/j.jpowsour.2024.234741.
[157] W.W. Ng, H.S. Thiam, Y.L. Pang, Y.S. Lim, J. Wong, Mater. Today Proc. (2023), https://doi.org/10.1016/j.matpr.2023.01.407.
[158] N. Samadi, M. Sabzi, M. Babaahmadi, Int. J. Biol. Macromol. 107 (2018) 2291–2297, https://doi.org/10.1016/j.ijbiomac.2017.10.104.
[159] L. Wang, S.G. Advani, A.K. Prasad, ECS Trans. 80 (8) (2017) 545, https://doi.org/10.1149/08008.0545ecst.
[160] C.F. Yunfa Dong, Haodong Xie, Yuhui He, Carlos M. Costa, Senentxu Lanceros-Méndez, Jiecai Han, Weidong He Inorganic Chem. Front. 11 (2024) 4459–4468, https://doi.org/10.1039/d4qi01074d.
[161] H. Zarrin, D. Higgins, Y. Jun, Z. Chen, M. Fowler, J. Phys. Chem. C 115 (42) (2011) 20774–20781, https://doi.org/10.1021/jp204610j.
[162] M.R. Asghar, W. Zhang, H. Su, J. Zhang, H. Liu, L. Xing, X. Yan, Q. Xu, Energy Adv. 4 (2) (2025) 185–223, https://doi.org/10.1039/D4YA00446A.
[163] F. Genç, N. Yıldırım Kılıç, M. Barsbay, ACS Omega 9 (26) (2024) 28194–28206, https://doi.org/10.1021/acsomega.4c01522.
[164] W. Heo, D.-H. Han, S.-J. Oh, J.U. Yoon, I. Woo, S.-E. Choi, J.-M. Yoon, J.W. Bae, J. Power Sources 642 (2025) 237010, https://doi.org/10.1016/j.jpowsour.2025.237010.
[165] Z. Kolská, A. Řezníčková, V. Hnatowicz, V. Švorčík, Vacuum 86 (6) (2012) 643–647, https://doi.org/10.1016/j.vacuum.2011.07.015.
[166] Y. Luo, X. Li, X. Zhang, J. Liu, X. Deng, ChemCatChem 16 (4) (2024) e202301372, https://doi.org/10.1002/cctc.202301372.
[167] J. Wang, Y. Dai, R. Wan, W. Wei, S. Xu, F. Zhai, R. He, Chem. Eng. J. 413 (2021) 127541, https://doi.org/10.1016/j.cej.2020.127541.
[168] S.-H. Shin, A. Kodir, D. Shin, S.-H. Park, B. Bae, Electrochim. Acta 298 (2019) 901–909, https://doi.org/10.1016/j.electacta.2018.12.150.
[169] S. Park, H. Lee, S.-H. Shin, N. Kim, D. Shin, B. Bae, ACS Omega 3 (9) (2018) 11262–11269, https://doi.org/10.1021/acsomega.8b01063.
[170] Y. Zhang, X. Tang, S. Xu, C. Sun, Deep learning-based state-of-health estimation of proton-exchange membrane fuel cells under dynamic operation conditions, Sensors 24 (2024).
[171] S. Tamilarasan, C.-K. Wang, Y.-D. Kuan, Y.-C. Shih, I. Stachiv, Renew. Sustain. Energy Rev. 226 (2025) 116274, https://doi.org/10.1016/j.rser.2025.116274.
[172] Z. Liu, S. Xu, H. Zhao, Y. Wang, Appl. Energy 326 (2022) 119975, https://doi.org/10.1016/j.apenergy.2022.119975.
[173] K. Jiang, Z. Liang, H. Jiang, T. Zheng, Y. Luan, Y. Feng, G. Lu, Z. Liu, Energy 336 (2025) 138449, https://doi.org/10.1016/j.energy.2025.138449.
[174] R. Ding, Y. Cheng, X. Fan, S. Mao, N. Wang, Int. J. Hydrogen Energy 58 (2024) 1514–1525, https://doi.org/10.1016/j.ijhydene.2024.01.309.
[175] P. Wang, H. Liu, J. Chen, X. Qin, W. Lehnert, Z. Shao, R. Li, Int. J. Hydrogen Energy 46 (61) (2021) 31353–31361, https://doi.org/10.1016/j.ijhydene.2021.07.004.
[176] F. Zhang, B. Zu, B. Wang, Z. Qin, J. Yao, Z. Wang, L. Fan, K. Jiao, Joule 9 (3) (2025) 101853, https://doi.org/10.1016/j.joule.2025.101853.
[177] F. Zhang, B. Wang, Z. Gong, Z. Qin, Y. Yin, T. Guo, F. Wang, B. Zu, K. Jiao, Next Energy 1 (3) (2023) 100052, https://doi.org/10.1016/j.nxener.2023.100052.
[178] F. Zhang, M. Ni, S. Tai, B. Zu, F. Xi, Y. Shen, B. Wang, Z. Qin, R. Wang, T. Guo, et al., Appl. Energy 384 (2025) 125483, https://doi.org/10.1016/j.apenergy.2025.125483.
[179] F. Zhang, X. Zhang, B. Wang, H. Zhai, K. Wu, Z. Wang, Z. Bao, W. Tian, W. Duan, B. Zu, et al., Digital Chem. Eng. 10 (2024) 100144, https://doi.org/10.1016/j.dche.2024.100144.